Mechanical Systems and Signal Processing 50-51 (2015) 757–783

Contents lists available at ScienceDirect

Mechanical Systems and Signal Processing

journal homepage: www.elsevier.com/locate/ymssp

Traceability of Acoustic Emission measurements for a proposed calibration method – Classification of characteristics and identification using signal analysis

James Griffin

University of Chile, Beauchef 850, Torre Central, Santiago, Chile

ARTICLE INFO

Article history:
Received 4 June 2013
Received in revised form
17 April 2014
Accepted 23 April 2014
Available online 28 May 2014

Keywords:
Single grit scratch tests
Acoustic Emission
Force
Time–frequency domain
Tensile tests
Signal analysis
Neural networks
Fuzzy-c clustering
CART rule based system and Simulink models

ABSTRACT

When using Acoustic Emission (AE) technologies, tensile, compressive and shear stress/strain tests can provide a detector for material deformation and dislocations. In this paper improvements are made to standardise calibration techniques for AE against known metrics such as force. AE signatures were evaluated from various calibration energy sources based on the energy from the first harmonic (dominant energy band) [1,2]. The effects of AE against its calibration identity are investigated: where signals are correlated to the average energy and distance of the detected phenomena. In addition, extra tests are investigated in terms of the tensile tests and single grit tests characterising different materials. Necessary translations to the time–frequency domain were necessary when segregating salient features between different material properties. Continuing this work the obtained AE is summarised and evaluated by a Neural Network (NN) regression classification technique which identifies how far the malformation has progressed (in terms of energy/force) during material transformation. Both genetic-fuzzy clustering and tree rule based classifier techniques were used as the second and third classification techniques respectively to verify the NN output giving a weighted three classifier system. The work discussed in this paper looks at both distance and force relationships for various prolonged Acoustic Emission stresses. Later such analysis was realised with different classifier models and finally implemented into the Simulink simulations. Further investigations were made into classifier models for different material interactions in terms of force and distance which add further dimension to this work with different materials based simulation realisations.

Within the statistical analysis section there are two varying prolonged stress tests which together offer the mechanical calibration system (automated solenoid and pencil break calibration system). Taking such a mechanical system with the real-time simulations gives a fully automated accurate AE calibration system to force and distance measurement phenomena.

1. Introduction

When machining aerospace alloys, there are a number of signal extraction technologies that can be used to identify the onset of malfunction which promotes efficient machining for the duration of manufacture. A key point to note here is the use of a calibration method that is both recorded and referenced to previous energy patterns. To ensure this process, information is recorded and interpreted and if a condition of concern is identified this must be evaluated in terms of its energy level and if further diagnosed as a concern, must then be acted on [3]. In contrast, AE is less established in industry

http://dx.doi.org/10.1016/j.ymssp.2014.04.018
0888-3270/

than other signals such as force, accelerations, strain, temperature, torque and power which are all internationally recognised standards where AE is not. This is difficult to do due to the nature of extraction where AE is sensitive to minute material dislocations and such measurements can differ significantly due to daily environmental changes such a temperature, air pressure and humidity to name a few. Such differences attribute to different signal time of flights, change of wave reflections, differences in material mediums and lastly, the difference in the process of calibration. The method presented in this paper ensures a correlation from known standardised phenomena to the less verified phenomena of AE.

Other sensors such as force are very useful for extracting workpiece deflection and even stiffness characteristics. Moreover, AE and force sensors look at similar conditions within the machining environment with importance being placed on the correct interpretation of the signal where different facets are extracted due to the different sampling frequencies used for the different sensing technologies. This paper will discuss all the AE signal representations against known phenomena.

Distance and force correlate very well for AE calibration when analysing the rich summarised extracted time signal; however to gain more useful information in terms of the material differences, a high bandwidth of AE frequency response needs to be identified and recognised. With rich information in the form of frequency band intensity it is possible to separate different material interactions exerting the same force at the same distance from the AE sensor(s). The method presented in terms of signal processing for preparation to the classifier uses a rich summary extraction technique to segregate time extracted signals in the form of the 5 highest peaks and the 5 lowest troughs and their associated time steps to the next proceeding zero point in time. This summary data technique is carried out for every 100 points of extracted data to give a 20 summary data points representation (5:1 compression ratio) which gives a rich summary of data (5 max, 5 min and 5 related times from the respective min–max points to the next zero point in time). This gives useful information in terms of both intensity and intensity to distance (hence the higher the frequency/amplitude components the closer the phenomenon). Such a technique is considered powerful and computationally affordable. If however there is more than one material being calibrated against then a more powerful technique is required which is more computationally demanding. Such a technique is one that translates the time to the time–frequency representations (such as Short-time Fourier transforms (STFT)) and segregates the different material interactions made by prolonged stress when applied to different materials. For a generic classifier system correlating force and distance of different materials extra frequency components from the STFT (5 max frequency peaks for that 100 points of time data) is added to the rich summary data information giving an even richer representation. The 20 points windowed summarised data is taken across every 100 points of the raw extracted AE signal and for the duration of average signal phenomena (1000 points of raw extracted AE signal).

The last section of the paper investigates intelligent models with Neural Network (NN) representations, Fuzzy clustering and tree rules based classifiers providing verified model predictions for distance and force when an AE source is emitted from prolonged stress. Further work in distinguishing signal phenomena for different materials is also discussed taking the time series summary representation further.

The main investigation objectives of this paper are

- Characterise the force and distance phenomenon in horizontal SG scratch tests.
- Characterise force and distance phenomenon using a rich summary signal pre/processing technique.
- Characterise AE to force and distance phenomenon for pencil break calibration tests.
- Characterise AE to force phenomenon for tensile tests.
- Characterise AE to force phenomenon for different material tests.
- Characterise and analyse AE in terms of statistical measurements for possible calibration technique: SG, pencil break and tensile tests.
- Characterise and analyse AE in terms of statistical measurements for possible calibration technique: varying intensities for pencil break and solenoid prolonged stress measurements.
- Verify signals with Dual AE sensors set equal distances apart and from sensor delay determine the position of the scratch interaction.
- Classify force and distance data using NN technique.
- Verify the classification process using training, test and verification data using fuzzy clustering and tree rule based classifiers.
- Produce AE to force and distance simulation displaying changing energy patterns as the prolonged stress changes in intensity (all the above objectives displayed within the proposed simulation).
- Produce AE to material distinction simulation displaying changing energy patterns from the same prolonged stress against different material mediums.

The remainder of this paper is organised as follows: Acoustic Emission technology (Section 2), Experimental Setup for AE calibration tests (Section 3), Acoustic Emission Analysis and Results (Section 4), Classifier Technologies (Section 5), Classifier Results (Section 6), AE Calibration Model Simulations (Section 7), Discussion of Results (Section 8) and Conclusions (Section 9).

2. Acoustic Emission technology

AE has been used for materials research in monitoring stresses from AE events emitted from crack initiation, structural defects, measurements, and other material anomalies. From such work it was found that most materials emit sounds or stress

waves as they are deformed; these sounds provide the very nature of plastic deformation under different intensities which inherently give warning signals for impending failure of a material. A lot of work in the area of AE has been made on many different materials from homogeneous/non-homogeneous metals/alloys to rocks and earth quake monitoring. The sensitivity of such sensors is of paramount importance, for example, when applied to single grit tests where the AE phenomenon is so minuet and localised it is difficult to detect and therefore there is a need for sensitivity. AE generated from material under stress refers to the generation of transient elastic waves during the rapid release of energy from the localised sources within a material. The difference between the AE technique and other non-destructive evaluation (NDE) methods is that AE detects the activities inside the materials, while other NDE methods attempt to examine the internal structures of the materials. Furthermore, AE only needs the input of one or more relatively small sensors fixed on the surface of the structure or specimen under examination.

AE sensors use crystals or certain ceramic materials which generate a piezoelectric voltage when a mechanical stress is applied. The deformation of the crystal is very small (0.1% of the original dimension). Such devices can be used to detect emitted waves, the generation of high voltages, electronic frequency generation, microbalance, and ultra-fine focusing of optical assemblies. When crystals are subjected to a change when being compressed, twisted or even distorted an electric charge is emitted and which is proportional to change in pressure/force. In short, when a load is applied to the sensing element, deformation of the crystal lattice exists which results in the generation of an electric charge [4,5].

In addition, bio-sensors and medical imaging (diagnostic ultrasound/medical ultrasonography) also use this technology which is very precise in terms of measurement and output. For good confidence levels in using AE technology, exhaustive tests are required to understand and define the limitations of operation.

The disadvantage of AE is that commercial AE systems can only estimate qualitatively how much damage is in the material and approximately how long the components will last. So, other NDE methods are still needed to do more thorough examinations and provide quantitative results (such as force and displacement sensors).

From tests carried out within this work there are noticeable oscillations and reflections of surface/material phenomenon apparent within the returned AE signal. Such oscillations are due to the size and thickness of the material, the level of energy emitted from the elastic/plastic deformation machining process, the distance between sensor, material anomalies and the material damping coefficient. Due to materials having different dimensions and characteristics there need to be more work concerning the stability and reliability and this is why other sensors are used to verify the signal analysis.

The AE wave is described as a non-stationary stochastic signal and this is why a continual wave stream is required as the short burst high frequencies can be missed with event driven methods.

AE sensor sensitivity is the ratio of pressure for each μbar from a given point of phenomenon and the open loop voltage caused by the sound pressure (piezoelectric effect). The sensors can be calibrated for either pressure waves (V/μbar) or with transient waves (V m/s) but they cannot be converted from each other once the calibration has been selected. The sensor has a maximum displacement of approximately 200 pm which is extremely sensitive when compared with atomic radii (atomic force microscope) with a range displacement of 150 pm. With these characteristics, AE is very useful for monitoring material processing.

2.1. Current work on AE calibration

AE is seeing more applications used in industry due to the possibilities to measure a change in minute phenomena; however calibration methods for such developing technologies have not been accepted in terms of standardisation and instead are only associated with best practices [6].

Hatano et al. [1] looked at pencil calibrations and various other calibration methods to investigate the AE elastic wave time/velocity and phase behaviour. Their investigation looked at both transmitted and received signals. During experiments, the actual test plate was measured in terms of its absolute dimensions and was considered flawless in terms of any possible machining discontinuities. Reciprocity calibration has been used in underwater acoustics [1]; however both Raleigh and longitudinal waves were measured from the AE event. The test pieces used in the work presented in this paper use the same dimensions for both distance and force measurements during pencil calibrations. However, this was not possible for machining SG and tensile tests and the method presented here looks at the recorded direct energy and correlated known phenomena in terms of distance and force. This is also summarised in [1] where spurious waves do not make a huge significance to dominant waves (Raleigh and longitudinal). In short, the AE elastic waves are located in terms of the dominant energy bands.

Yan et al. [2] discussed a calibration method to be used in connection with the primary sensor. This is where a piezoelectric point source emitter and known material for the contact plate resulted in an accurate calibration method from the initiation of an artificial AE source. This technique is limited to structures of a certain width and the material being used for machining is required to be the same as the backing sensor plate. In addition, the self-calibration method discussed by Yan et al. [2,7] is essentially a method to measure the coupling capacity of the AE sensor through the initiated back plate artificial AE source. In short, a sensor monitoring another sensor in-situ where the first sensor initiates the artificial test calibration pulse for second sensor to pick-up (both transmitted and received signals) similar to the work presented in [1,2].

Goding et al. [8] look at using k-means and self-organising maps (SOM) which are similar to fuzzy-neural classifiers in segregating different mechanisms of material failure referenced to tensile tests and the recorded AE signals, where such AE is reduced in terms of n-dimensionality to give the rise time, peaks and, the counts of threshold passes. Similar research is reflected in this paper where a similar process is used; however the peaks and troughs time to the zero is considered a more salient characteristic and is particularly useful for classification. This reduction technique coupled with the Short Time

Fourier Transform (STFT) summarised information has not been seen in AE calibration literature before and has been found to be a powerful method to promote segregation based on different signal characteristics.

3. Experimental setup for AE calibration tests

This paper obtains its results from a near noise free environment; however as previous research [9] has displayed with the use of filters such signals obtained during harsh environments can be used against known calibrated signals and used for monitoring the onset and the continuation of material failure. The work presented here uses a number of different signals obtained during various experimental tests and the addition of calibration tests made during machining trials to compare and use against. Current work in the arena of AE calibration is discussed.

The proposed work outlined in this paper is based on work discussed by Hatano [1] where intelligent correlation is made from the signal input/output to the classifier which essentially is a three layer NN. Also, with more sensors present, the dominant signals can be measured in terms of transmitting and receiving the amplitude, phase and velocity.

There were two experiments carried out for this work, the first consisted of pencil break tests to gain the time of flight (see future sections for more information) and different intensities experienced at different sensor distances (see Fig. 3a and b for experimental setup). The second looked at various AE emitted sources from prolonged stress with correlated force relationships which consisted of three tests: SG tests (see Figs. 1 and 3 for setup and future sections for more information), pencil break calibration tests and finally, the AE experienced during tensile tests of super aerospace alloys (see Fig. 2 for set-up information).

The other being distance which has proved to be accurate over short distances (1–200 mm) when comparing with previous methods [10]. Therefore both experiments supply rich information for a calibration standard when measuring AE sources. Both data collected from the two experiments is then reduced in terms of dimensionality (see section AE system and tensile tests) and presented to two independent NN for expert classification. Such a regime would be combined for production methods; however it was necessary to display the two facets of information. Figs. 1 and 2 display the set-up for the three individual tests reference to the first experiment set: (1) SG, (2) pencil calibration. The SG experiments give micro-force and AE relationships for micro-induced intensities which are below and approaching that of pencil calibrations and finally tensile tests. Fig. 3a illustrates the distances for pencil calibration and force tests. The SG experiments were designed to gain the relationship between AE and force (both low and high forces) where the distances were measured and recorded and finally, for tensile tests, the two sensors were kept 10 mm apart.

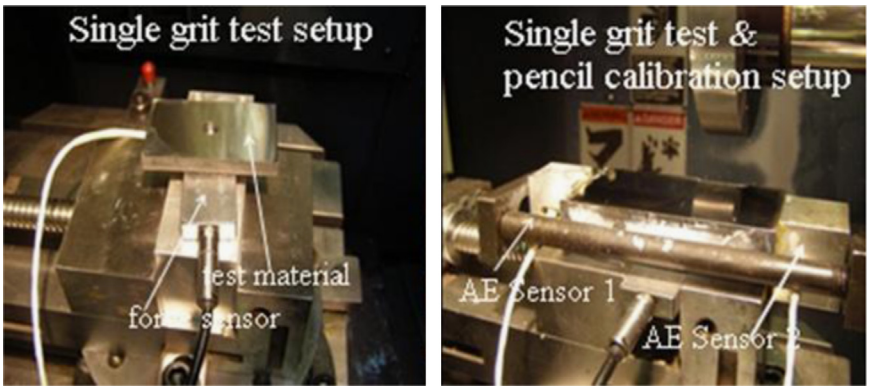

Fig. 1. Pencil break and single grit experimental setup.

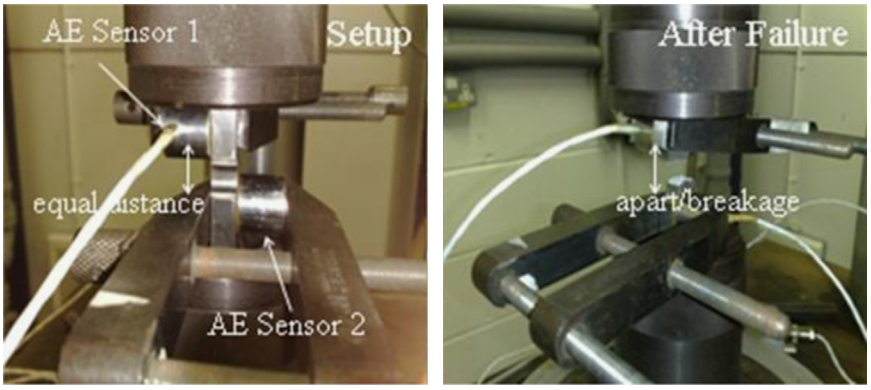

Fig. 2. Tensile tests for AE vs. force using both non/machined super alloy workpieces.

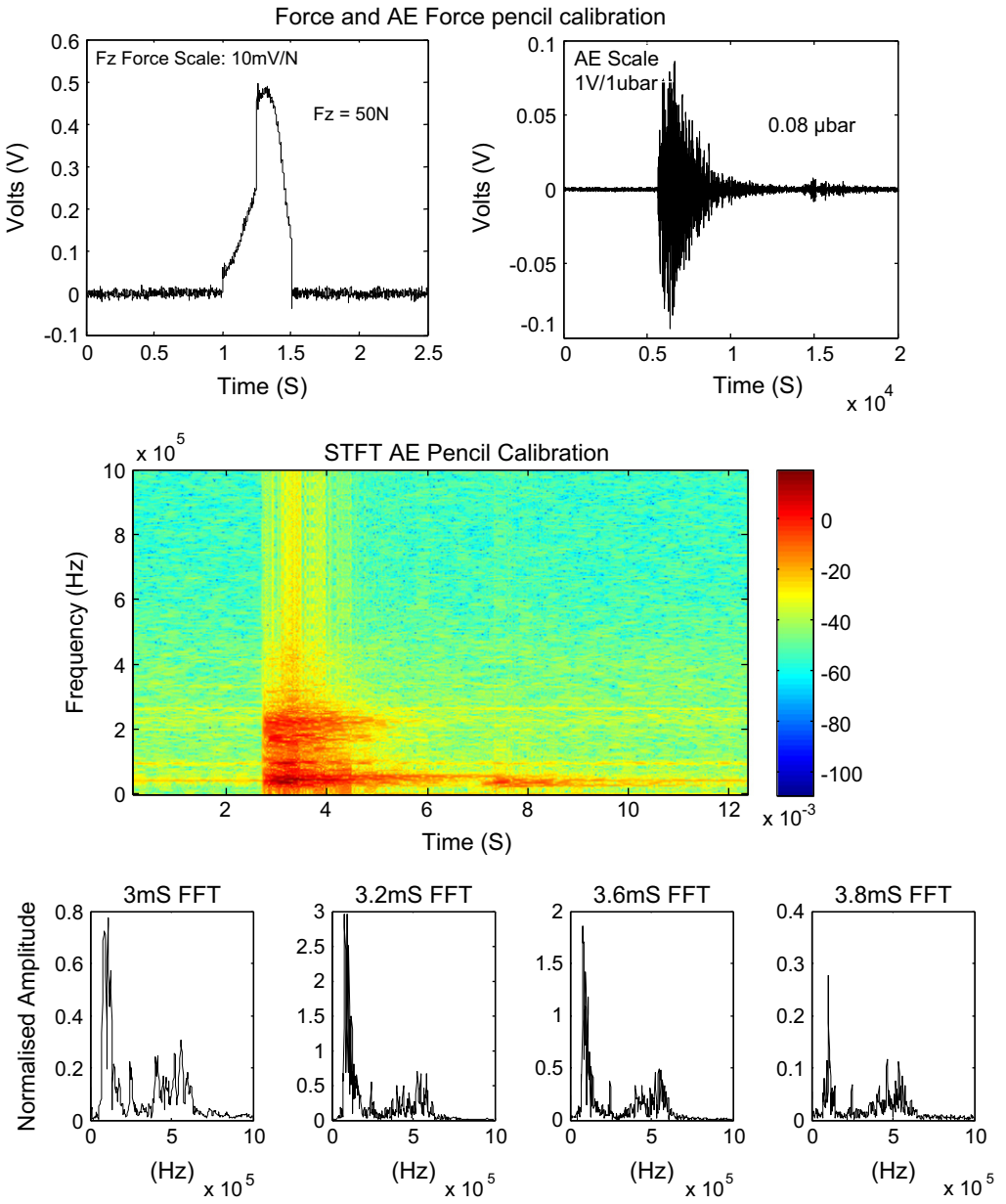

Fig. 3. TOP: Force and AE Pencil Break, MIDDLE: STFT and BOTTOM: Fast Fourier Transform (FFT) Slices of STFT.

The experiments information is tabulated in Table 1 as experiment numbers 1 and 2 and such experiments were specifically looking for different intensities and force between two AE sensors (sensors 1 and 2) by changing the distance of the pencil break calibration tests (Hit1, Hit2 and Hit3).

The data obtained by both experiments can be used for calibration conversion to the known standard. In addition other measured phenomena such as the force experienced in tensile and SG tests are also considered. Essentially the classifier gives a translation from AE to a known measurable phenomenon.

4. Acoustic Emission analysis and results

4.1. Acoustic Emission oscillation and time of flight

Acoustic energy waves occur naturally when matter vibrates at a frequency usually between 1 Hz and 600 kHz [11]. Acoustic energy can be described as sound which has a range between 20 Hz and 20 kHz and can be detected by the human ear. Lower frequency acoustic energy has a long wavelength and takes a longer period of time to attenuate. The converse is

Table 1
Experimental setup information for time of flight pencil break calibration tests using dual AE sensors.

Experiment number	Experiment fibre break (hit) number	Sensor 1 distance from break (mm)	Sensor 2 distance from break (mm)	Experiment type
1	1	120	20	Comparison near/far
1	2	140	40	Comparison near/far
1	3	160	60	Comparison near/far
2	1	20	10	Near AE source
2	2	30	20	Near AE source
2	3	50	40	Near AE source
3	1	220	120	Far AE source
3	2	240	140	Far AE source
3	3	260	160	Far AE source

true for higher frequency acoustic energy, where a shorter wavelength exists and therefore a shorter period of time to attenuate. For instance, a low note played from a piano lasts much longer than high note.

The AE experienced from the applied stress of either grinding or SG scratch tests experiences damping which can be quantified in terms of a material damping constant for the emitted AE energy. It can be noted that if the material [12] is brittle in nature, the damping coefficient is much less than if the material is more ductile and thus experiences hardly any oscillations. Following on, the signal amplitude and damped oscillations decrease steadily relative to the material characteristics. Such oscillations add to the retrieved signal phenomenon thus suspending the propagation of dislocations in time. The oscillations contain important material information and should be noted when correlating the physical material characteristics with the extracted AE signal phenomenon. In addition to the material characteristics, the fixture and the grit materials also play an important role in the AE material damping coefficient, where the stiffer the experimental set-up, the less oscillations will be allowed to vibrate around the material medium [13,14].

To see the differences in time of flight for the AE to return from the crack position of the pencil break, an experiment was set up as tabulated in Table 1reference experiment 3. This was to see the difference in rise of signal over the norm (background noise with no AE emission). This would prove the subtle differences of the returning AE to the receiver reference to the fracture of the pencil break. In addition, this experiment displays how sensitive the AE sensor was for the experiments discussed in this paper [15].

4.2. Pencil calibration

In addition to SG tests, two specially designed tests look at the energy and distance relationship where pencil calibrations were used for obtaining additional measurements. Every time machining would be carried out, a pencil calibration test would be made ensuring the sensor is correlated to a specific noise level and operating normally based on previous historical data. This test however would not normally be correlated to a distance or force measurement. This calibration check ensures a fair and accurate comparison between the signals. The pencil break tests can suggest if the sensitivity has been set too high or low and may saturate during machining. The proposal in this paper is for the user to take five calibration measurements with an automatic pencil and with outliers ignored (based on possible variance spread) it would be possible to automatically calibrate against known data stored in a Neural Network (NN) to gain both distance and force relationships. Such known quantities can be stored in combination with the AE recorded data and used for monitoring defects as well as legal requirements for condition/health monitoring.

The pencil break method is a manufacturing practice used for AE sensor calibration purposes. The simulated AE method is known as the Hsu–Heilsen source (breaking of a high polymer graphite pencil lead to provide a localised AE burst [6]) which provides a broadband step-release transient wave. Important factors to take into consideration are the length of the lead, lead diameter, lead hardness and angle of application between the lead and the surface of the workpiece, as these factors affect the frequency and amplitude of the extracted signal [13].

The sensor is required to be clamped as close as possible to the phenomenon of interest. The closer the sensor: the less time of flight, reverberations and signal reflections. The current best practices specify a 2H lead of 0.5 mm diameter, 3 mm length should be used for the pencil calibration. Such a signal is displayed in Fig. 3. Fig. 3 shows a pencil break and force extracted signal displaying the calibration between force and the AE emitted stress. The calibration was carried out at 10 mm away from the AE sensor.

4.3. Pencil calibration to recognise time of flight and distance

As shown in Fig. 6 the STFT image gives the energy intensities of the extracted AE source and predominately what one is interested in, such signals are summarised in terms of richness with both peak and trough time to zero calculations.

This section looks at pencil calibration tests and various AE source recordings. These specifically are based on varying distances with two clamped AE sensor microphones (see Table 1 for details of set-up information). Fig. 4 displays a

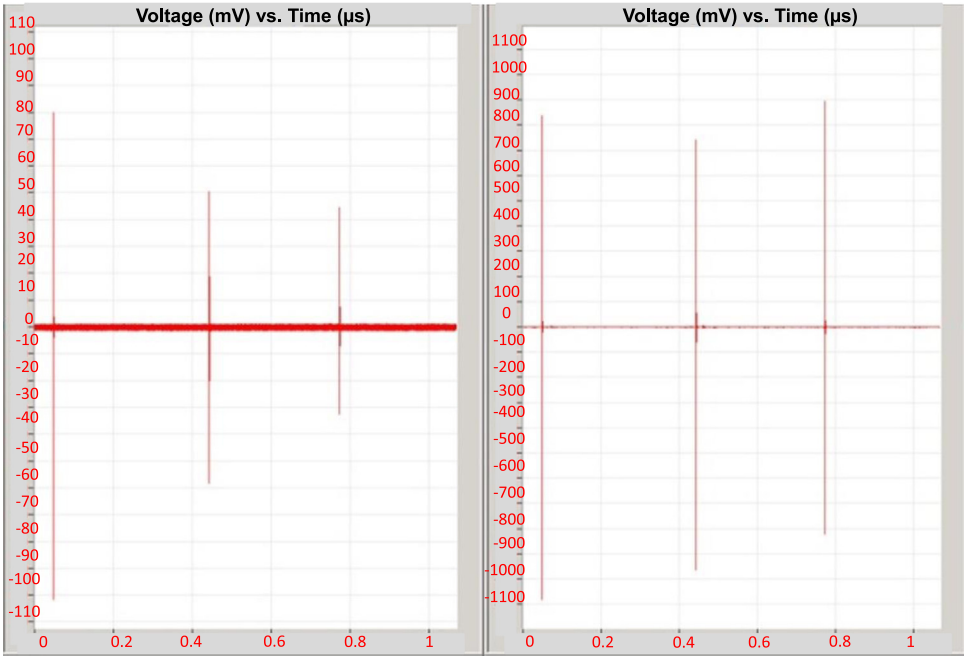

Fig. 4. Pencil break time of flight/intensity experimental waveviewer results.

waveviewer screen capture of three pencil calibration sources, at the various distances taken by a two sensor set-up as displayed in Fig. 1 and information tabulated in Table 1.

4.4. Single grit tests

For the SG test [16] a piece of single grit (SG) was glued into a microscopic drilled hole of the specially designed steel plate. The steel plate would then be fixed to the spindle and rotated at the same range of commercial grinding speeds. The SG was fixed to the plate in a protruding fashion which would ensure the SG was the first object to make contact with the workpiece when controlled within a micron of accuracy. The machine set-up also consisted of the AE and force sensors being attached in a manner to ensure maximum signal extraction. For monitoring the force and AE, two computers were synchronised by switch driven digital acquisition cards.

The scratch test was carried out by feeding a rotating Al_2O_3 grit towards a flat horizontally placed workpiece (see Fig. 1). With a micron incremental grit stroke, a scratch groove will be formed on the surface of the flat sample. The average scratch depth is about 1 μm, which is a typical value of grinding chip in high efficiency grinding. During a single scratch action the AE feature frequency bands/intensities change with respect to time significant of different applied forces. In short, the mechanical AE propagation should be considered in both time and frequency features.

An AE data acquisition system where two Physical Acoustics WD AE sensors were used both identical and with a frequency response range of 80 kHz–1 MHz. The two sensors were set-up equal distances apart (see Fig. 1 for set-up configuration). The sampling rate was set to 5 MHz to ensure no aliasing occurred when the signal was reconstructed using the Matlab Digital Signal Toolbox (DSP) and all the short burst high frequency information was obtained.

Fig. 5 displays the raw extracted time AE signal (TOP) followed by its STFT representation (middle) and the Photomap 3D measurement image (bottom). Looking at the figure, the phenomena displayed by the STFT/time representations of AE hit correlate to a measured cut length of 401 μm (SG scratch length for the contact phenomena). The interaction between grit and workpiece takes 14 μs which is calculated from the following equation:

$$v_g = \frac{\pi D\, RPM - v_w}{60} \tag{1}$$

where v_g is the grain cut through speed, wheel rotational speed in *RPM* is 4000 RPM, the diameter *D* of the steel wheel on which the grit is glued upon is 138 mm and the test piece feed speed v_w is 4000 mm/min. The calculation of v_g gives a very fast peripheral grain cut through speed of 28,836 mm/s. Such tests were carried out to see the effects of the relationship between AE and force.

Pencil break tests [4] also displayed a large response time to what can only be described as a microsecond fracture. Fig. 5 displays the STFT of the SG tests which is significant when displaying the energy intensities against that of the known force phenomenon (including the material interaction).

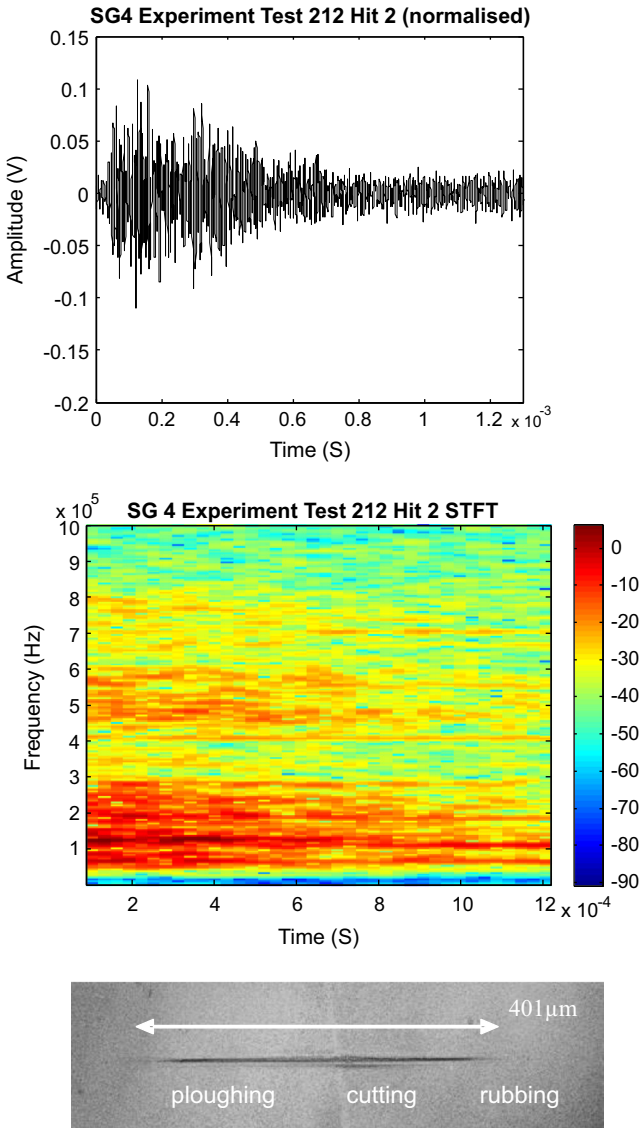

Fig. 5. TOP: Time extracted AE signal, MIDDLE: STFT and BOTTOM: Photomap image of grit interaction.

The aforementioned experiments were carried out to give different correlations between AE and force for changing phenomena. This builds the gap between pencil calibrations and tensile tests in promoting more data for regression purposes in classification.

4.5. Tensile tests

Figs. 6 and 7 display the AE time and STFT representations of the tensile test experiment using aerospace super alloy test pieces (similar in nature to Inconel 718). As shown in Fig. 8 the AE time source displays a relationship of 4 V to 4 μbar of recorded shear pressure this relates to 0.7 mm of tensile movement and therefore 17.5 kN of force.

The STFT displayed in Fig. 7 displays the correlated energy intensities of emitted AE during the tensile tests of super alloys. Here the energy has significant frequency bands at 300 and 800 kHz which are significant to mechanical stress and heat changing properties [9,14].

The AE energy patterns within these tests were reduced in terms of n-dimensionality where the richness of data was used for both classification and training data. The n-dimensional reduction technique is a computationally inexpensive method where the first five highest peaks and the lowest troughs would be found along a specified window of raw extracted signal length and each of those peaks/troughs would have its time taken from the peak to the next zero state. Such information would be windowed along the raw time extracted signal. For every 100 points along an average signal length of a 1000 points extracted signal equates to 20 points of summary windowed information. Therefore for every window of

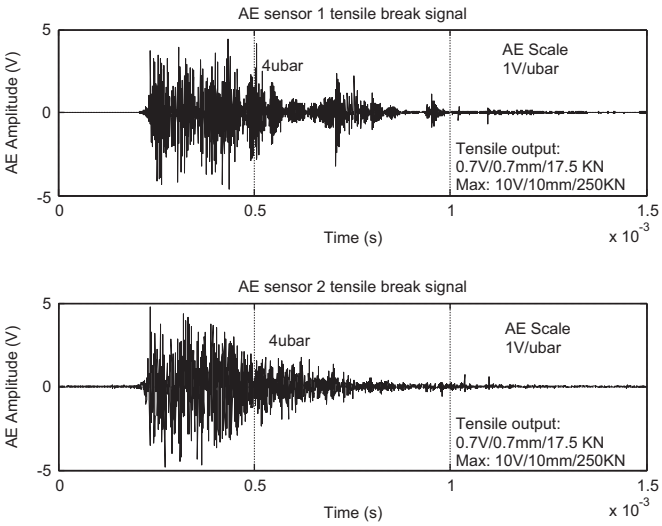

Fig. 6. Tensile test AE signal at point of material failure.

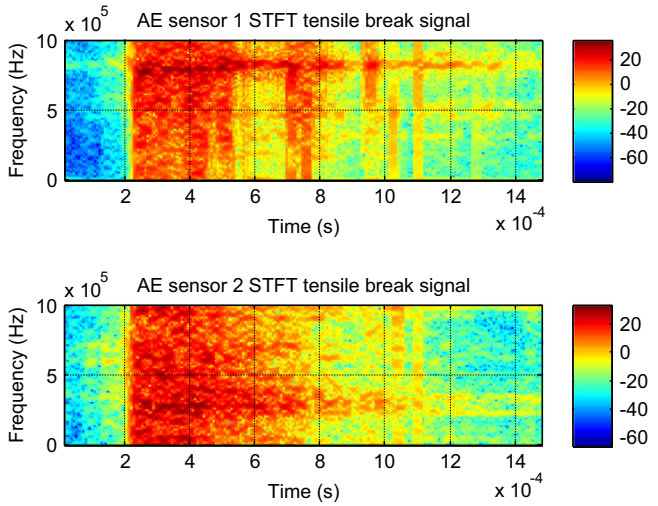

Fig. 7. Tensile test AE STFT signal at point of material failure.

extracted 100 points, the 5 largest peaks and troughs would be found and recorded along with their respective time from peak to the next proceeding zero state.

This technique was considered to be very useful as the results can easily be transferable to real time applications and at the same time, give a rich summary account of the signal phenomenon. These tests would be weighted in terms of the mean value for a given five samples. If outliers were found (based on variance of the extracted signals) they would be ignored and the mean level amount being based on the signals within a set tolerance of variance. This mean oriented way of calibration can then be checked against a database for both phenomena in terms of distance and force intensities. It was felt that the techniques presented here are paving the way forward for an accepted method of calibration in AE. The database weights would be changed accordingly with more verified data added at some later point in time.

4.6. Single grit material interaction tests

This section investigates SG material interactions where the same force and distance is exerted during tests. This information provides another dimension to AE calibration techniques in that first distance and force measurements are useful for a single material; however, if different materials are being calibrated against then the addition of another classification technique is required. To separate the different material signals using time–frequency analysis through the use of STFT allows the translation from the first method of using the rich summary time series information providing both the time and frequency domains representation. Figs. 8 and 9 display different AE extracted signals and their respective frequency–time domain STFT representations for different materials.

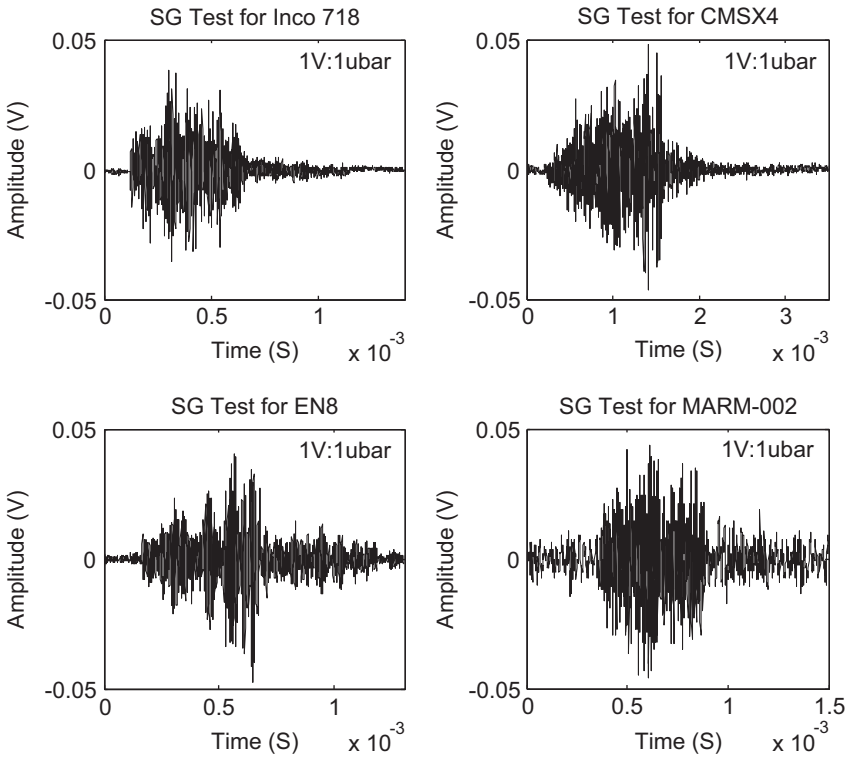

Fig. 8. AE SG events for Inconel 718, CMSX4, EN8 and MARM-002 materials.

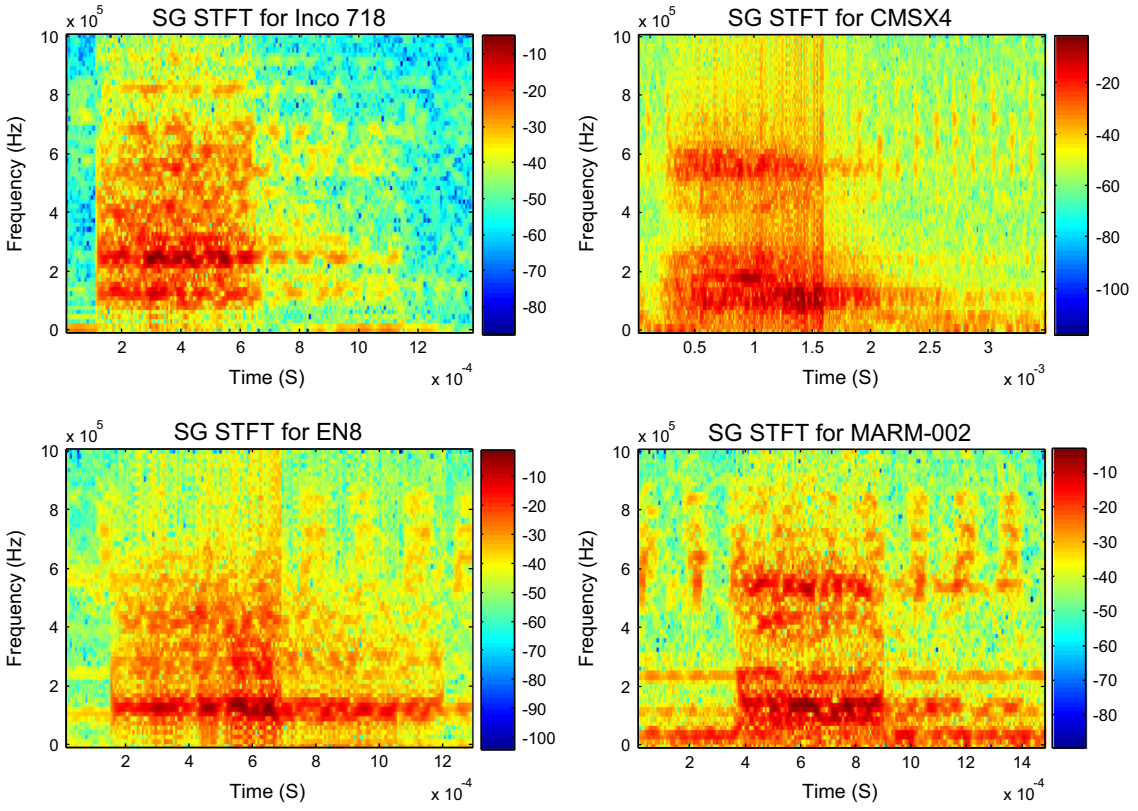

Fig. 9. AE STFT for Inconel 718, CMSX4, EN8 and MARM-002 materials.

Table 2
Aerospace material properties used in this work [18].

Property	Inconel 718	CMSX4	EN8 Steel	MARM-002
Composition (wt%)	Mo: 3, Cr: 18, Ti: 0.9 Nb: 5.1, Fe: 18.3, Ni: 53.7	Mo: 0.6, Cr: 7, Ti: 1, Al: 5.6, Co: 10 Ni: 67, Re: 3, W: 6	C: 0.36–0440, Mn: 0.6–0.1, S: <0.05, P: 0.04	Co: 8.25 Cr: 5.5 Ni: 59 W: 10, Ta: 3.0, Ti: 1.0, Al: 5.5, Mo: 0.7, Fe: 0.5, B: 0.015
Density (kg/m^3)	8193	8690	7800–8030	8267
Hardness (HV)	456	520	178	470
Tensile strength (MPa)	758–1407	1090	510–660	965
Yield strength (MPa=N/mm^2)	1150	1150	245–530	815
Yield strength (MPa=N/mm^2)	1150	990	245–530	815
Elastic modulus (GPa)	31	18.5	200	24.6
Elongation (%)	21–27	10–12	32.8	13–17
Melting point (°C)	1336	1395	950	1130
Poisson's ratio	0.284	0.273	0.29	0.295
Thermal conductivity (W/mk)	11.4–28.7	12–63	60.5	33.5
Special heat capacity (K/kg K)	430–700	381–544	437.2	450
Thermal diffusivity ($\times 10^{-6}$ m^2/s)	2.01–8.24	2.54–21	17.74	16

As shown in Figs. 8 and 9 it can be seen that higher intensities at low frequency bands (100 kHz) are prominent for all the materials tested with greater intensities for materials with greater levels of hardness (see Table 2). Looking at the mid frequency signature bands of the material EN8 steel, this is the only material that does not have high intensities when compared with other super alloy, nickel based materials. The nickel based super alloy materials have higher levels of hardness than that of EN8 steel and therefore requires more energy to create material dislocations. Differences in material compositions can be seen between all the materials as shown in Fig. 13; Inconel 718 had prominent bands at 250 and 400 kHz, CMSX4 had prominent bands between the 100, 200, 600 and 650 kHz, EN8 had prominent bands at 200 kHz and finally, MARM-002 had prominent bands between 150, 525 and 575 kHz. These segregations of frequency bands give the capability to classify different AE material signatures when faced with the same stimulated force at a specified constant distance [17].

4.7. Acoustic Emission statistical tests

This section looks at statistical and regression analyses to verify the suitability of the various forms of AE when exerted to different prolonged stresses. Due to the miniscule measurement difficulties with some tests, some test sets are small in nature however still give an indication of general tendencies (pencil calibration and single grit tests with force). In addition, it was difficult to make many tensile tests and therefore such data is small in nature but still gives a general indication of possible spread. This section looks at various statistical tests for the following: pencil break tests (amplitude change with respect to distance), solenoid hit tests (amplitude change with respect to distance), tensile tests (amplitude change with respect to force), pencil break tests (amplitude change with respect to force) and single grit tests (amplitude change with respect to force). The solenoid/pencil break distance tests follow the same setup as pencil break distance setup described in Sections 4.1–4.3. Both tests combined give a good varying analysis of AE over distance. Combined further with the AE to force tests gives a possible mechanical solution for an automated AE calibration technique.

Figs. 10 and 11 investigate the pencil break and solenoid amplitude tests with respect to changing distances (experiment setup information tabulated in Table 3). Tables 4 and 5 give the statistical and regression measurements for both tests respectively. Voltage amplitude instead of power decibel amplitude was considered more sensitive to change and therefore communicated here (where the measurement conversion was set up to be 1 V per 1 μbar of pressure).

Looking at the data in Fig. 10 and Table 4 it can be seen that the general patterns signify that the amplitudes decrease as the distance increases (see mean measurement in Table 4). In addition the standard deviation spread increases as the distance increases; therefore it will be implied that as the distance significantly increases the measurements become more variable and questionable. However the distances chosen in this work look at maximum distances with small variation which are suitable for miniscule measurement.

The data presented in Fig. 11 and Table 5 reinforce the pencil break tests with respect to distance. Here two sets of parallel tests were carried out to give more verification for a possible automated calibration method where a combined pencil break and solenoid system can exist, in-situ within the sensor. The forces experienced with the clamped solenoid to workpiece setup gave similar forces to pencil break calibration tests between 45 N and 50 N (see Fig. 15 for pencil break calibration and force tests).

Again the solenoid tests give similar results to the distance pencil break tests where the amplitude deceases as the distance increases. Giving similar verification the standard deviation spread is also noted as similar. For a proposed automated calibration system there would be a lot less variability in a purpose built system and therefore an adapted solenoid pencil break calibration system would give more improved results.

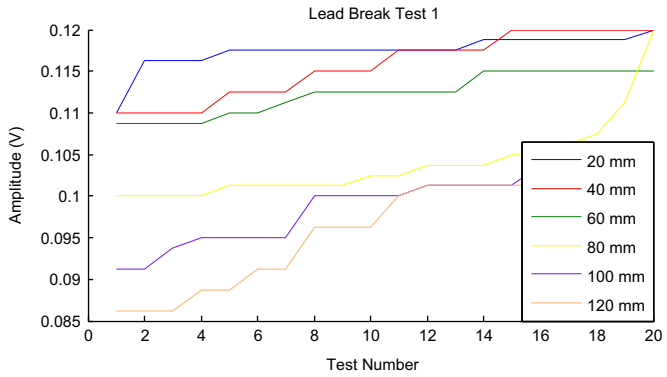

Fig. 10. Acoustic Emission distance tests using pencil lead fibre break tests.

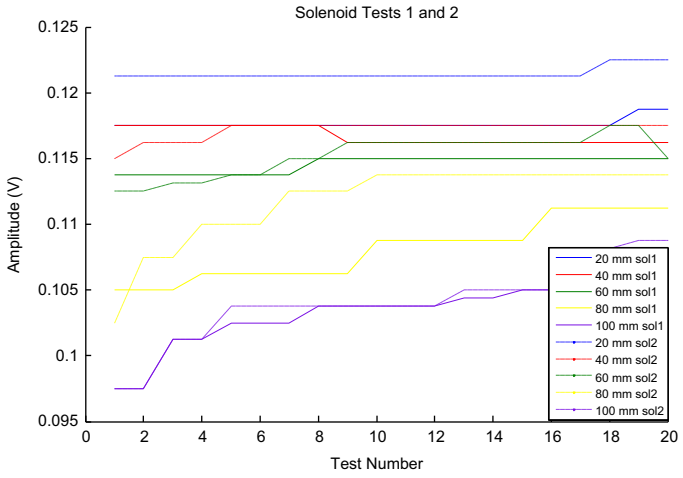

Fig. 11. Acoustic Emission distance tests using Solenoid hit tests.

Table 3
Experimental setup information for incremental pencil break calibration tests.

AE experiment number	Experiment fibre break number	AE Sensor distance from break (mm)	Experiment type
4	1	20	Pencil Incremental AE source
4	2	40	Pencil Incremental AE source
4	3	60	Pencil Incremental AE source
4	4	80	Pencil Incremental AE source
4	5	100	Pencil Incremental AE source
4	6	120	Pencil Incremental AE source
5	1	20	Solenoid Incremental AE source
5	2	40	Solenoid Incremental AE source
5	3	60	Solenoid Incremental AE source
5	4	80	Solenoid Incremental AE source
5	5	100	Solenoid Incremental AE source
5	6	120	Solenoid Incremental AE source

With the aerospace material tensile tests it was difficult to carry out many tests (reference Fig. 12 tensile tests) however such tests display there is an increase in amplitude (V) as the force increases. In addition such data gives the higher end of amplitude and force measurements for an automated AE calibration classification system. For the tensile tests the distance between both sensors was equal and the material plastic deformation phenomenon was located in the same position (note standard tensile test specimens were used).

Figs. 13 and 14 display the AE pencil break and single grit tests respectively which were correlated with force measurements (prolonged stress initiated at the same distance). Due to difficulties [19] in obtaining force measurements for

Table 4
The linear line equations and statistics for Fig. 12.

Distance (mm)	Mean	Std dev.	Linear line equations
20	0.1174	0.002006	$y=0.00025x+0.11$
40	0.1156	0.003879	$y=0.00064x+0.11$
60	0.1123	0.002443	$y=0.0004x+0.11$
80	0.1039	0.00478	$y=0.00066x+0.097$
100	0.09919	0.004521	$y=0.00074x+0.091$
120	0.09613	0.006255	$y=0.001x+0.086$

Table 5
The linear line equations and statistics for Fig. 11.

Sol test	Distance (mm)	Mean	Std dev.	Linear line equations
Sol 1	20	0.1176	0.0003847	$y=3.4e-5x+0.12$
Sol 1	40	0.1167	0.0006283	$y=9e-5x+0.12$
Sol 1	60	0.1146	0.0006117	$y=8.6e-5x+0.11$
Sol 1	80	0.1081	0.002311	$y=0.00037x+0.1$
Sol 1	100	0.1034	0.002528	$y=0.00039x+0.099$
Sol 2	20	0.1214	0.0004579	$y=4.8e-5x+0.12$
Sol 2	40	0.1172	0.0006876	$y=7.8e-5x+0.12$
Sol 2	60	0.1153	0.001589	$y=0.00023x+0.11$
Sol 2	80	0.1118	0.003048	$y=0.00042x+0.11$
Sol 2	100	0.1041	0.003105	$y=0.00048x+0.099$

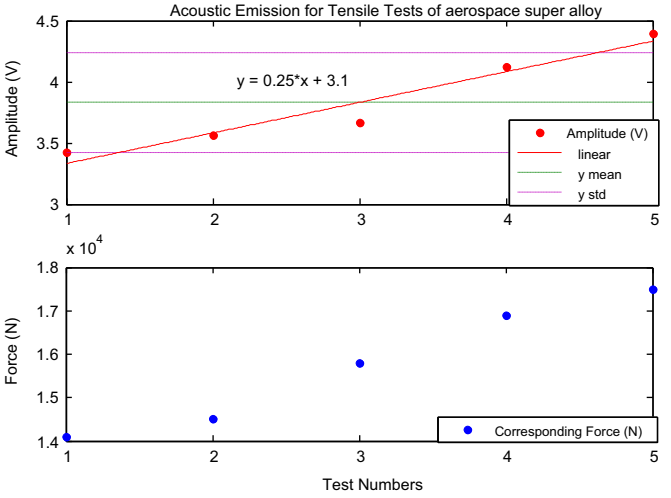

Fig. 12. Tensile tests with acoustic emission and force.

single grit tests, the test set displayed in Fig. 14 is small however general trends are displayed. From both tests it can be seen that as force increases so does the received amplitude voltage. The pencil break tests have less variability due to similar initiated prolonged stress from the pencil break fracture [6] when compared to the single grit tests. The single grit tests have more variability as the beginning and end of the scratch grooves are significant of less force (maximum force is achieved when approaching the negative apex of the scratch groove). Lastly from looking at different STFT images of measured AE with respect to changing distances it was noticed that higher frequencies and higher amplitudes were recorded near AE phenomenon when compared with lower frequencies and lower amplitudes with AE phenomenon further away. This is an important consideration for an automated classification system and is further reinforced from the commonly known that power is inversely proportional to frequency (see Figs. 3 and 4 where the higher frequencies have the less intensity compared to the lower frequencies where both low and high frequencies are significant to the most intense part of the prolonged stress).

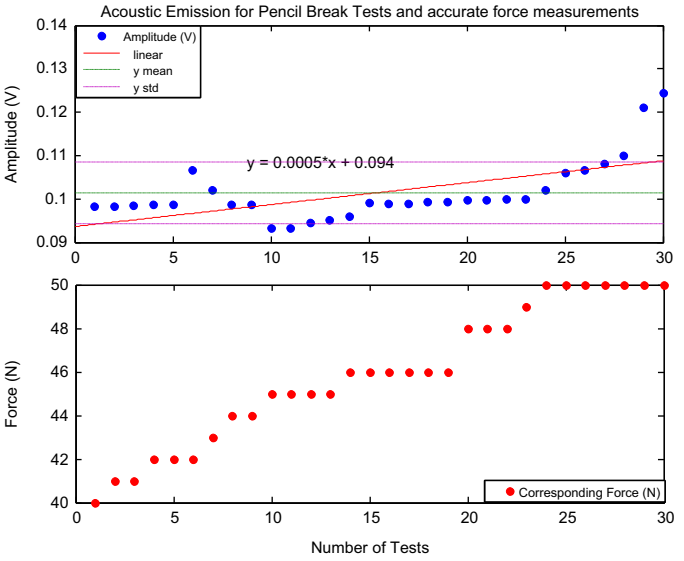

Fig. 13. Pencil break tests with acoustic emission and force.

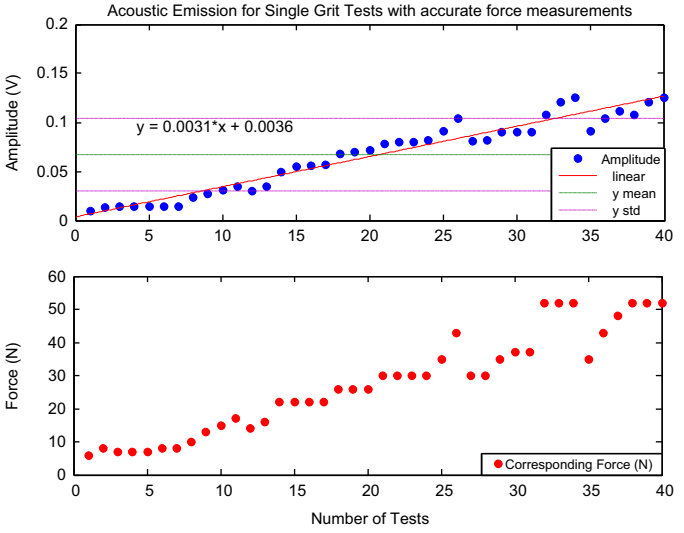

Fig. 14. Single grit tests with acoustic emission and force.

5. Classifier technologies

5.1. Neural networks for classification of calibration data

A large number of researchers have reported the application of using NN models for the classification of phenomena of interest when applied to tool condition monitoring [20]. A feed-forward NN model was used with the back-propagation learning strategy to provide the segregation of data [21]. Commonly, NNs are used for pattern recognition in image analysis or sound waves in signal analysis. The NN consists of a complex interconnection of units which are otherwise known as nodes or neurons. The general layout for a NN consists of a set of neuron layers connected together through complex connections; this layout and features are known as the network architecture.

The transfer function (for non-linear problems a differential transfer function, such as Tan-sigmoid is used) is required to map the non-linear input–output relations which are obtained for each neuron and updated in an iterative fashion towards the desired target set. Back-propagation is so called as the weights are updated from the error between the actual output and the desired output which in short is from the back to the front of the network topology. This method segregates the different classes based on the supervised training data given to the NN. The summation of weights and bias values is multiplied by a differential transfer function to give a neuron output.

Table 6
NN parameters for NN classifications.

NN parameters	Value
Hidden layers	1
Input size	200 Neurons of rich AE time series
Transfer function for layers	I/P: TAN, 2nd: TAN, O/P: PURE
Epochs	16,000
Learning rule	Back-propagation (step size: 10^{-9})
Momentum	0.9

The output of each neuron is a function of its inputs. Specifically, output of the *j*th neuron is reference to the specific layer and is described by the following equations:

$$U_j = \sum(Pi^* w_{ij}) \tag{2}$$

$$a_i = F(U_j + t_j) \tag{3}$$

For every neuron, '*j*', in a layer, each of the '*i*' inputs, P_i to that layer is multiplied by a previously established weight, w_{ij}. These are all summed together, resulting in the internal value of the operation, U_j. This value is then biased by a previously established threshold value t_j, and sent through an activation function, F (Tan-Sigmoid or Linear) giving the NN output, a_i.

Eq. (4) describes the output error obtained from each neuron:

$$ME = \frac{1}{\Omega}\sum_{i=1}^{\Omega}(t_i - a_i)^2 \tag{4}$$

where ME is the mean squared error, a_i is the output of the network corresponding to *i*th input P_1–P_n. The error term of network is given from $(t_i - a_i)$ where t_i is the target vector or the desired value for given input vectors P_1–P_n. The error function can be applied to the NN in a batch training fashion at the end of data presentation or sequentially after each input–output pair.

For the back-propagation algorithm the weight and bias update equations are as follows:

$$\Delta w_{ij}^k = -\alpha\frac{\partial ME}{\partial w_{ij}^k} \tag{5}$$

$$\Delta b_i^k = -\alpha\frac{\partial ME}{\partial b_i^k} \tag{6}$$

where α is the learning rate, which has a trade-off in value to ensure it is small enough to gain a true convergence but large enough to separate the data space in adequate time. Eqs. (5) and (6) are iteratively changed across the network along with other functions to provide learning sensitivity. This process of weight and input, and error calculation propagates through the NN to provide the segregation rules which separates the data according to class (target vector). The '*b*' is a bias term used to influence the training weights and for NN training. Table 6 tabulates the NN parameters used in these tests.

5.2. Clustering method for classification of calibration data

Another pattern recognition technique used for classification is through Fuzzy clustering [22,23]. Pattern recognition can select features of interest based on all data features. The technique of fuzzy clustering provides rules in the form of distance measurements that segregate the different cluster sets from each other, in this case, AE vs. force and distance.

Clustering techniques have emerged from work carried out in statistical probability [24]. When looking at real world phenomena most cases are not finite and instead possess a lot of in-between values such as that seen in fuzzy sets. Fuzzy clustering-mean algorithm is an iterative technique for clustering data sets in a soft rule set fashion. It is a technique for grouping data and finding structures in data. Essentially clustering techniques use a distance measure to segregate like data from other presented data into classes or sets (clusters).

There are two main types of clustering techniques: the conventional way of clustering through hard clustering where partitions are formed representing each pattern similar to a threshold measure used for pre-processing the NN outputs. The difference in hard clustering is the data belongs to only one cluster. With nonlinear data there is no sharp classification between clusters, especially at the boundaries; this is why fuzzy clustering is better than other clustering techniques as it can assign clustering between 0 and 1 and not just one fixed value, therefore giving cases for both cluster sets. The classification here is based on the input data set and has more similarities when compared with the others and is known as soft clustering.

Fig. 15 displays a block diagram of the fuzzy-c/GA which is based on work carried out by [21] clustering AE vs. force and distance measurements. The first step in this process is to convert the rich reduced data-set and form the fuzzy similarity matrix defining the relations of similarity. The next process is to then define the fuzzy variable similarity matrix which

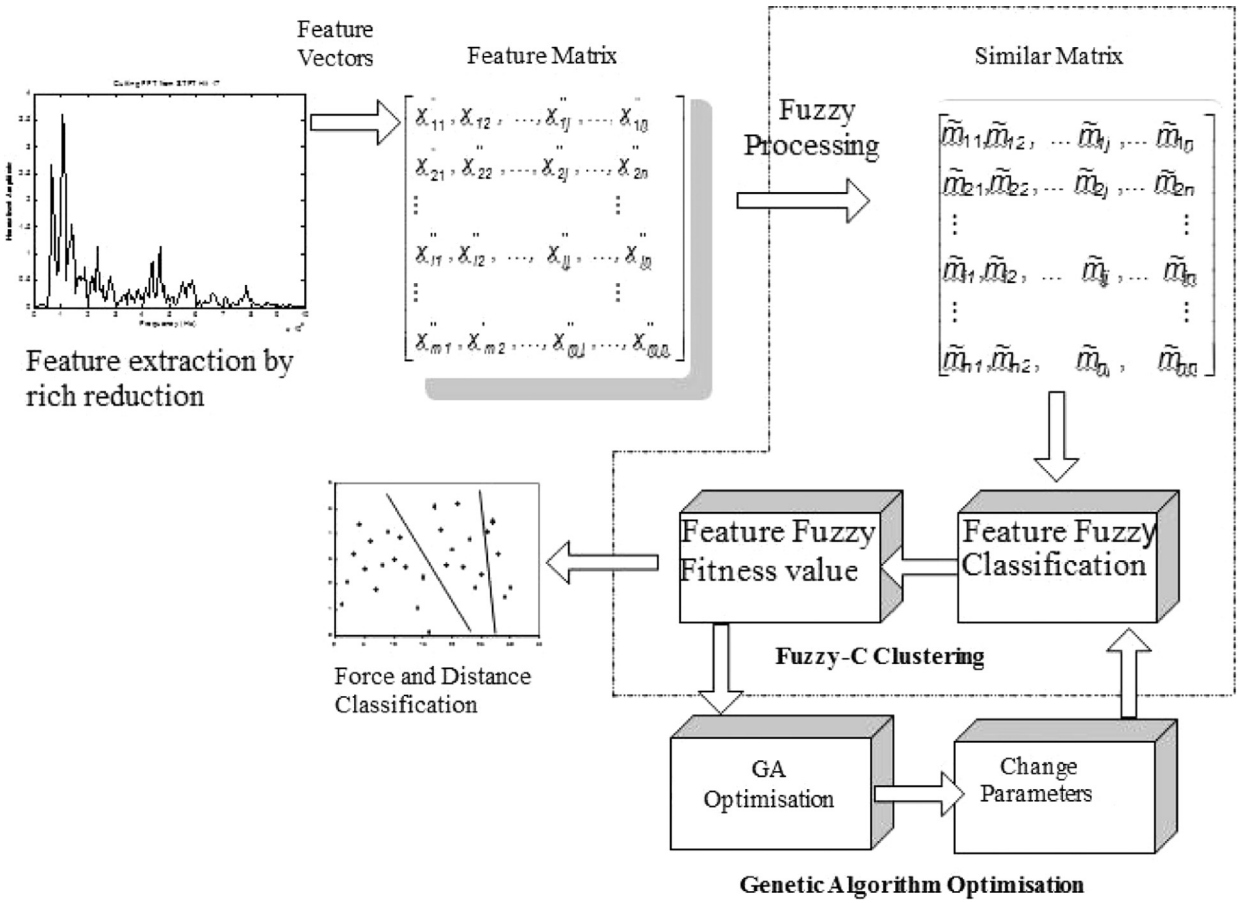

Fig. 15. Block diagram of Fuzzy-GA classification for AE vs. force and distance classifications.

evaluates each coefficients $\tilde{r}_{ij}$ degree of membership between the element i and element j. Following on, the cluster centres are determined, the centres segregate and categorise one cluster from another. The centre cluster is the representing function of a particular cluster set. Input test data that has a membership close to a particular centre than other centres means that input data belongs to that centre.

Let $X = \{X_1, X_2, \ldots, X_m\}$, $X \subset V$, where X_1 to X_m are feature vectors which make up the total feature matrix set and $X_i = (X_{i1}, X_{i2}, \ldots, X_{in}) \in V$ is a feature vector (element of total feature matrix set V); X_{ij} is the *jth* feature of individual X_i where feature matrix is made up from 1 to n feature vectors. To ensure there is normalisation across the feature matrix, Eq. (7) is used which calculates the normalised mean for each input value divided by the variance.

$$x'_{ij} = m_j X_{ij} \;\&\; x''_{ij} = (x'_{ij} - \overline{x}'_i)/\sigma_i \tag{7}$$

where

$$m_j = \max(X_{11}, X_{12}, \ldots, X_{1n})/X_{1j},\ \overline{x}'_i = \frac{1}{n}\sum_{j=1}^{n} x'_{ij} \;\&\; \sigma_i = \left|\frac{1}{n}\sum_{j=1}^{n}(x'_{ij} - \overline{x}'_i)^2\right|^{1/2}$$

The normalised feature matrix is then represented by the feature matrix:

$$X(m \times n) = \begin{bmatrix} x''_{11}, & x''_{12}, & \ldots, & x''_{1j}, & \ldots, & x''_{1n} \\ x''_{21}, & x''_{22}, & \ldots, & x''_{2j}, & \ldots, & x''_{2n} \\ \vdots & & & & \vdots & \\ x''_{i1}, & x''_{i2}, & \ldots, & x''_{ij}, & \ldots, & x''_{in} \\ \vdots & & & & \vdots & \\ x''_{m1}, & x''_{m2}, & \ldots, & x''_{mj}, & \ldots, & x''_{mn} \end{bmatrix} \tag{8}$$

The Fuzzy similarity matrix is the next calculation required for the fuzzy clustering of the input data set. The similarity

matrix uses a distance measure to show similarities within the matrix set. There are many distance functions available; however fuzzy-c clustering uses Eq. (9). The index of similarity is based on the minimum distance that equates to the maximum similarity.

$$m_{ij} = \frac{\sum_{k=1}^{n} |(x_{ik} - \overline{x}_i)(x_{kj} - \overline{x}_j)|}{\left\{ \left[\sum_{k=1}^{n} (x_{ik} - \overline{x})^2 \right] \cdot \left[\sum_{k=1}^{n} (x_{kj} - \overline{x}_j)^2 \right]^{1/2} \right\}} \tag{9}$$

By using the correlation coefficient Eq. (9) the normalised feature matrix is converted into a fuzzy proximity matrix M:

$$M = \begin{bmatrix} m_{11}, & m_{12}, & \ldots, & m_{1j}, & \ldots, & m_{1n} \\ m_{21}, & m_{22}, & \ldots, & m_{2j}, & \ldots, & m_{2n} \\ \vdots & & & & \vdots & \\ m_{i1}, & m_{i2}, & \ldots, & m_{ij}, & \ldots, & m_{in} \\ \vdots & & & & \vdots & \\ m_{m1}, & m_{m2}, & \ldots, & m_{mj}, & \ldots, & m_{mn} \end{bmatrix} \tag{10}$$

The fuzzy proximity matrix M is then converted into a fuzzy similarity matrix M^K as the proximity relationship does not have enough similarities for fuzzy clustering to be carried out. From using the fuzzy algorithm such as transitive closure, the fuzzy matrix M can be converted into the fuzzy similarity matrix M^K.

$$M^K = \begin{bmatrix} \tilde{m}_{11}, & \tilde{m}_{12}, & \ldots, & \tilde{m}_{1j}, & \ldots, & \tilde{m}_{1n} \\ \tilde{m}_{21}, & \tilde{m}_{22}, & \ldots, & \tilde{m}_{2j}, & \ldots, & \tilde{m}_{2n} \\ \vdots & & & & \vdots & \\ \tilde{m}_{i1}, & \tilde{m}_{i2}, & \ldots, & \tilde{m}_{ij}, & \ldots, & \tilde{m}_{in} \\ \vdots & & & & \vdots & \\ \tilde{m}_{m1}, & \tilde{m}_{m2}, & \ldots, & \tilde{m}_{mj}, & \ldots, & \tilde{m}_{mn} \end{bmatrix} \tag{11}$$

$$\min\left\{ J_m = \sum_{j=1}^{m} \sum_{i=1}^{n} |\mu_j(x_i)|^b ||x_i - c_j||^2 \right\} \tag{12}$$

Looking at Eq. (11), $\tilde{m}_{ij}$ in the matrix M^k is the similarity between feature 'i' and feature 'j.' The maximum value of similarity is when $i=j$ and the feature itself equates to 1. After ranking the features in the order of similarity values, it is then possible to segregate these features using the closest cluster distance membership function and distinguish the AE data in terms of force and distance measurements. The closest distance membership function of fuzzy-clustering is based on the squared loss cost function (see Eq. (12)) for each point. For Eq. (11), x_i is the samples ($i=1, 2, \ldots, n$), m is the number of known clusters, c_j is the cluster centre point where ($j=1, 2, \ldots, m$), and $\mu_j(x_i)$ is the fuzzy membership of sample x_i to cluster 'j.' The 'b' term if equals 1, tends more towards k-means clustering, similar to city-block distance statistical measure and if 'b' tends towards ∞ it becomes completely fuzzy similar to Chebyshev maximum distance clustering. If however the term 'b' takes the value of 2 it is similar to the Euclidean distance technique which was used in this work. The fuzzy algorithm iterates through Eq. (11) until it can no longer best fit the separation of one cluster from another.

5.3. Tree rule based systems for classification of calibration data

Rules can sometimes be a simple yet affective way to represent the classification of a given dataset. As the third classifier this is merely a third check on the two previously discussed technologies and it is easily formed into simulation test code as "if, else-if or else" rules. Such a method uses an interactive approach to segregate the data using discriminate values of more than or less than to give either a class or node to another rule or class. This type of classifier technique has not been used much in condition monitoring however it is referenced here as being used to classify the generation of rules [25] which is of particular importance to work presented in this paper in that the different classifiers verify one another's output.

Classification and Regression Trees (CART) however is a method of classification similar to fuzzy clustering with the added facet of producing more transparent rules which is why it has been used here to verify the output classifications of other classification technologies and it is easily transportable to real-time simulation. As mentioned before CART is also suitable for n-dimensional datasets which is what is presented here.

CART builds classification and regression trees for predicting continuous dependent variables (regression) and categorical predictor variables (classification). It achieves its functionality by recursively splitting the feature space into sets of non-overlapping regions, and finally by predicting the most likely value of the dependent variable within each region. By generating a binary tree through recursive partitioning it splits the data into sub nodes based on the minimisation of a heterogeneity criterion computed at the resulting sub-nodes. With the CART algorithm the tree is forwardly propagated (using forward stepwise regression) for best purity of node split. The best node split becomes the chosen value of partition (see Eq. (13)).

A good splitting criterion is the following:

$$PRE = \varnothing(s,t)$$

$$\text{Misclassification error: } Q_m = \frac{1}{N_m} \sum_{x_i \varepsilon R^m} (yi \neq k(m)) = 1 - \hat{P}_{mk(m)} \tag{13}$$

where y_i is the output of the individual under test and $k(m)$ is the class category under test.

PRE is the minimum production reduction in error, s is the spilt at any t node. The best purity measure looks at the best unique class classification where less impure looks at more multiclass representation. For the CART algorithm the percentage accuracy of classifications is used as the best purity measure [26].

This method of classification is not only chosen to verify fuzzy clustering/NNs and rule transparency but also because the tree fitting methods are actually closely related to cluster analysis [27]. This is where each node can be thought of as a cluster of objects, or cases, that are split by further branches in the tree. Note that the top node covers the whole sample amount and each remaining node contains a sub amount of the original sample and so on as the split levels increase.

A classification tree represents a set of nested logical if–then conditions (similar to a rule based system) on the values of the feature variables that allow the prediction of the value for the dependent categorical variable based on the observed values of the feature variables. A regression tree also represents a set of nested logical if–then conditions on the features variables, but these are used instead to predict the value of a continuous response variable.

CART can handle missing values by imputing such values in obtaining the mean over the complete observations. The model can be tested on a separately specified test set. Additionally, the model can be saved and used subsequently on additional test sets.

Some points for discussion on best tree representations are as follows:

- A very large tree may over fit the data.
- A small tree might not capture the important structure.

Therefore there is trade-off consideration for the best tree when thinking of the overall size:

- The optimal tree size should be adaptively chosen from the data provided.
- Different stopping criteria can give different results such as an impurity threshold is reached and the branching and splitting is halted or a specified minimum of branch level is achieved as so branching and splitting is halted at this point.
- Think of a pruning strategy that does not impact on the overall tree classification accuracy.

6. Classifier results

Fig. 16 displays the results made from first experiment where an accuracy of 93% classifications was obtained with half the cases unseen. Even the misclassifications (shown by the red boxes) appear to have the correct classification distinction albeit the level is lower than desired. For training, 150 test cases were used. This initial experiment displayed the possibility for such an automatic calibration method for AE against known quantities of force.

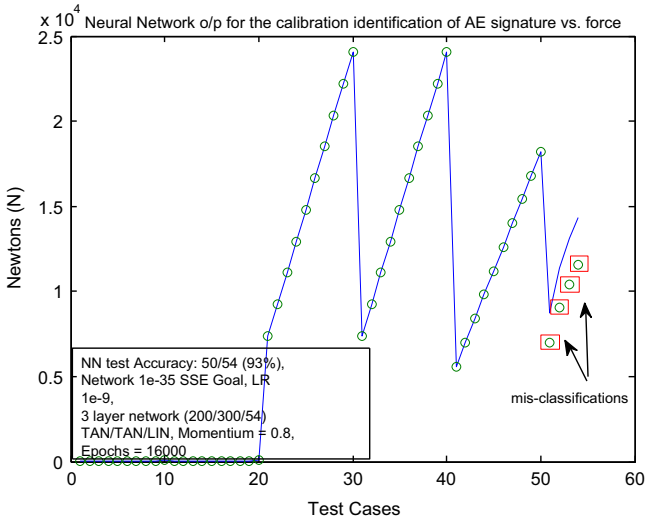

Fig. 16. Neural Network AE vs. force calibration results. (For interpretation of the references to colour in this figure legend, the reader is referred to the web version of this article.)

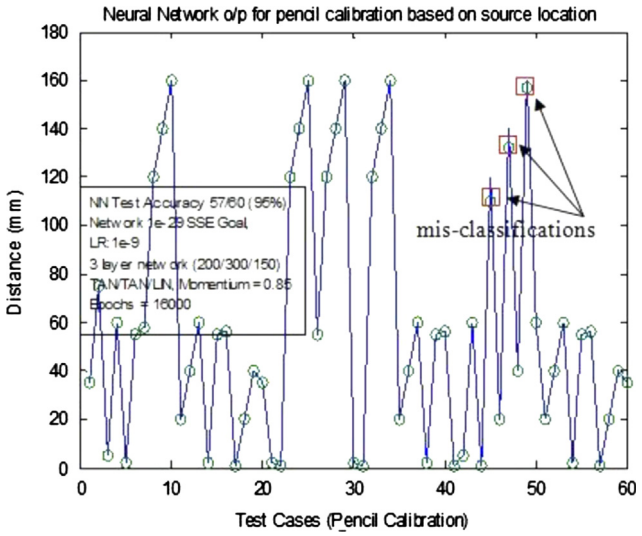

Fig. 17. Neural Network calibration results for AE source location. (For interpretation of the references to colour in this figure legend, the reader is referred to the web version of this article.)

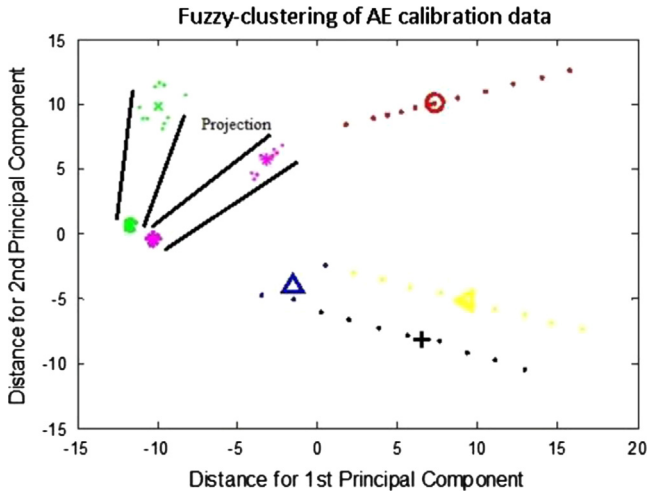

Fig. 18. Fuzzy-c/GA clustering results for AE vs. force.

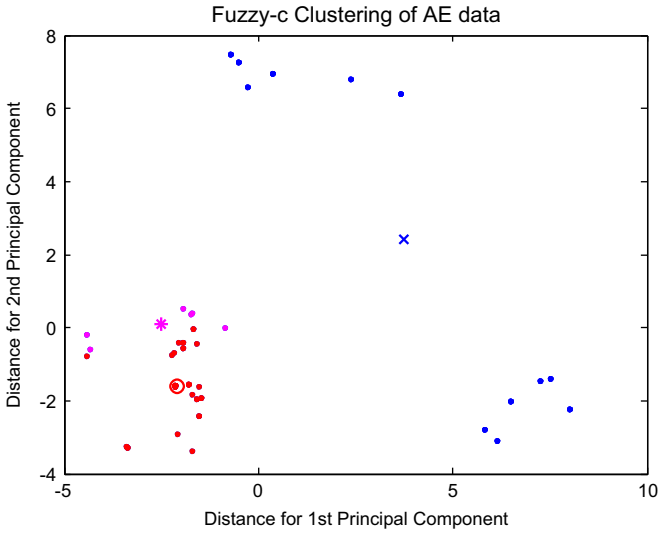

Fig. 19. Fuzzy-c/GA clustering results for AE vs. distance.

Fig. 17 displays results for the second experiment where results are similar to the first experiment with 95% accuracy. Again the unseen cases were 50% of the test data and again the misclassifications (shown by the red boxes) were correct just with an incorrect level difference. NNs are particularly good at giving multiple outputs and this is why such a classification technique was used during these experiments. The results display an indication that AE calibration can also be correlated to distance, based on the intensity of the measured signal.

This second classification technique verifies the NN results. Fig. 18 displays the results for the second experiment with 92% accuracy and Fig. 19 with 94% accuracy (unseen cases were 50% with respect to both test data sets). It can be said that NNs are more accurate for giving multiple outputs when compared with fuzzy-c cluster analysis. However with more training and test data this may not be the case. The tree based rules gave a further verification accuracy of 95% accuracy for both distance and force tests (where again the unseen cases were 50% of the test data set). Such verified results from various classifier technologies give a high confidence for such an automated calibration system. To verify the data, individual statistical tests were carried out in Section 4.7: AE statistical tests. Here high confidence was achieved for the majority of tests and as the classifiers act as regression classifiers both force and distance could be realised with a mix of calibration data (where the mix of data is considered more difficult to separate when compared with the individual AE tests (reference Section 4.7).

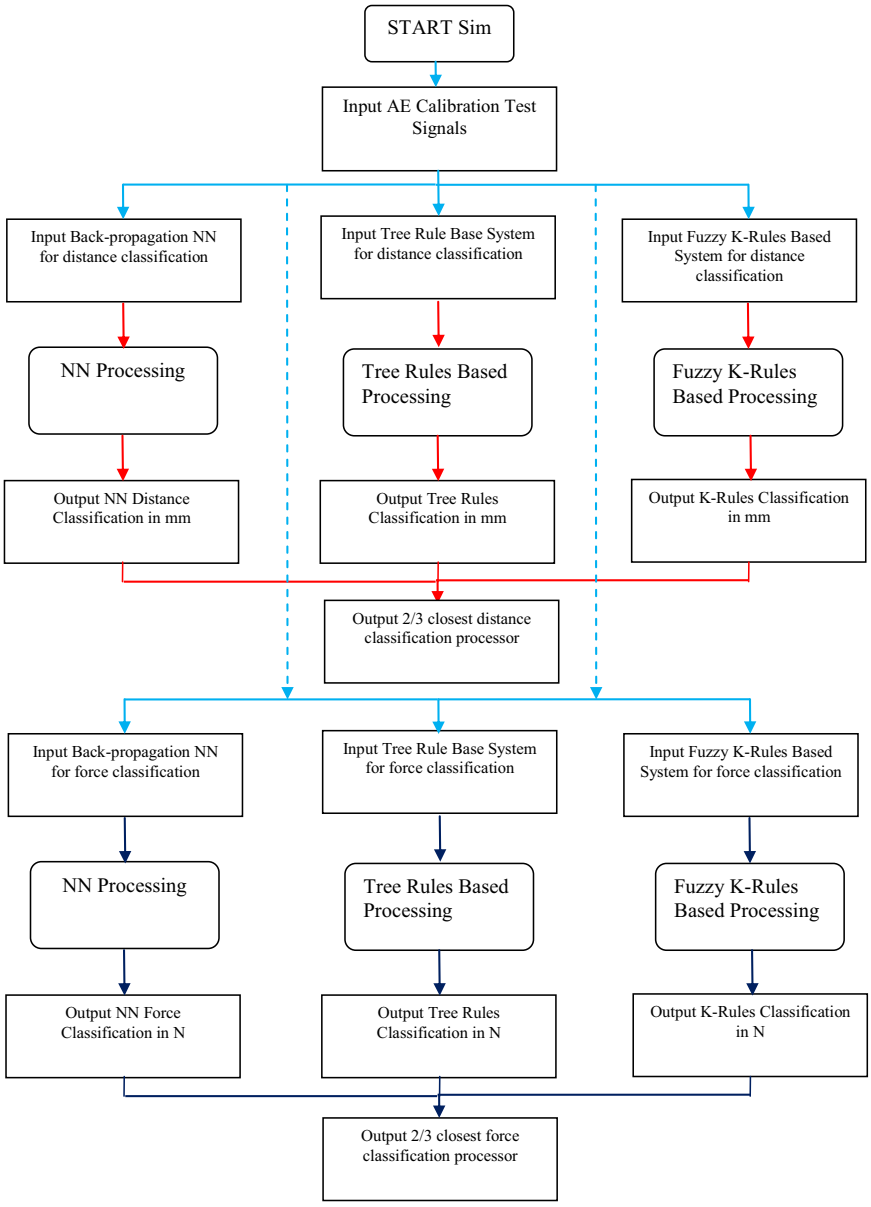

Fig. 20. Flow chart of Acoustic Emission calibration system.

7. AE calibration model simulations

The investigation of this section continues the work discussed in the first part where the classifier technologies along with other classifier technologies are discussed and realised in a Simulink model. In the second part further Simulink models realise classifier technologies for discriminating different materials when experienced with the same force and distance emitted AE sources.

7.1. Simulink model for AE calibration against distance and force

In the section of classifiers technologies and classifiers results, NNs and Fuzzy-C/GA clustering were discussed and used to provide results in discriminating AE against both distance and force calibrations. This section will introduce the NN, tree rule based system classification technique and the Fuzzy-clustering NN through radial basis distance function in the form of technologies realised into a real-time simulation.

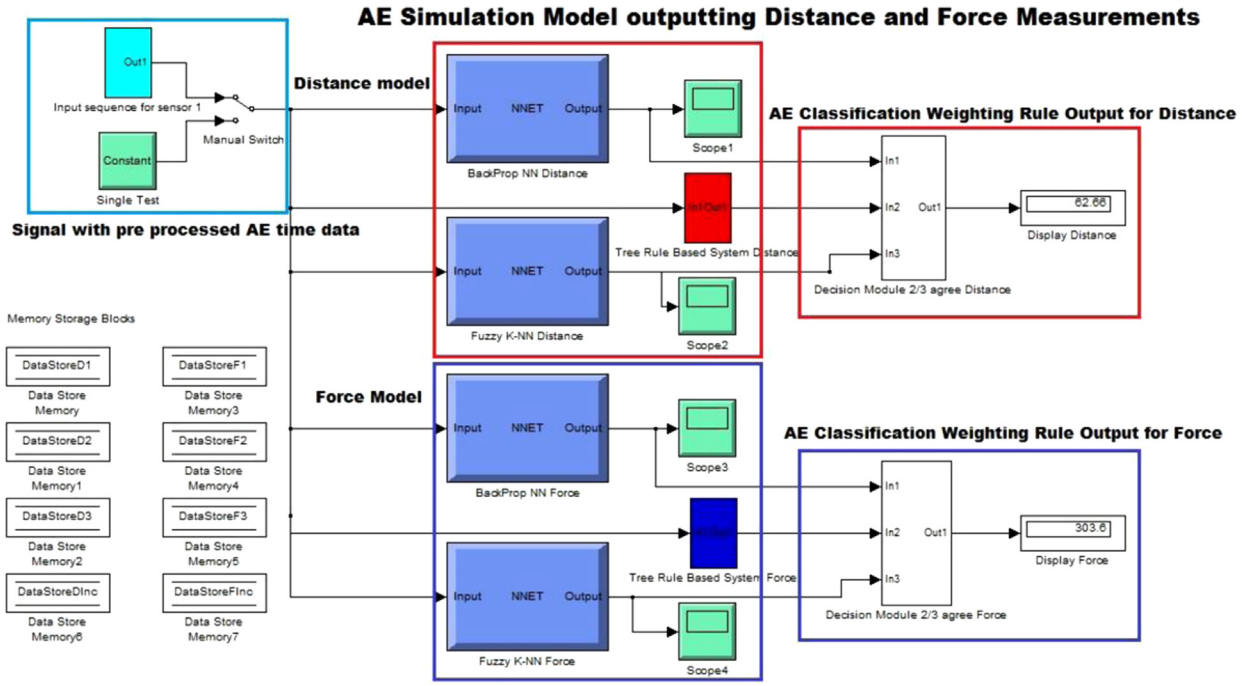

Fig. 21. Top level Simulink model for AE to distance and force calibration.

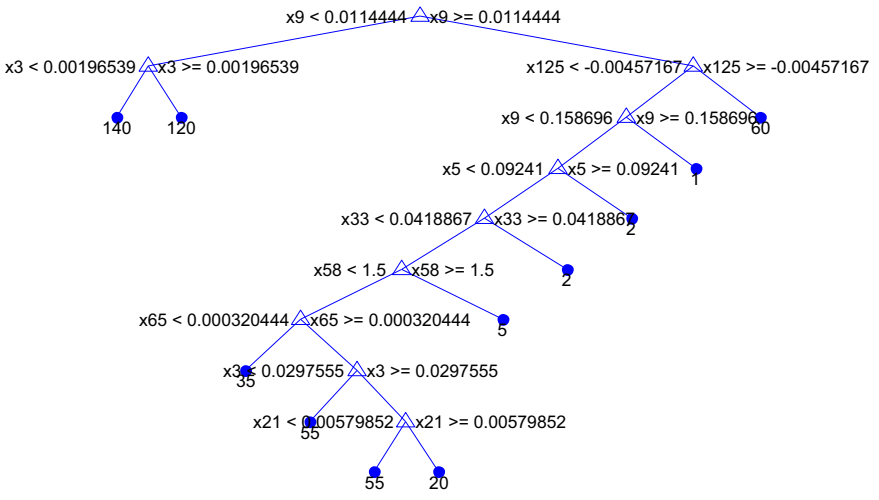

Fig. 22. Tree based rule system for distance classifications.

Fig. 20 displays the AE calibration process flow chart; here it can be seen the signal under test is checked against both distance and force expert systems for an associated output. Fig. 21 displays the full AE calibration simulation system, where the three agreeing expert decision classifications give a weighted output for calibration against a known standardised phenomena. As shown in Fig. 21 further, the left displays the method of testing five AE pencil calibration signals, the mid-top displays the 3 expert systems which are weighted towards classification accuracies and used to give accurate classification associations when faced with new AE phenomena. Here the classification is correlated against distance phenomena and output accordingly. The mid-bottom displays 3 expert systems which are again weighted towards classification accuracies with correlations to force phenomena and again, output accordingly.

The Simulink top level model displayed in Fig. 21 uses a three decision process for AE calibration against distance and another three below for AE calibration against force. The first classifier mimics the NN with Backpropagation weight learning rule. The second classifier uses a tree rule based system where the rules are translated and implemented into embedded Matlab script. The final classification technology gives a fuzzy clustering technique through a Kohonen NN with distance radial basis as a learning discriminator.

Fig. 22 displays the tree rule based output for the relationship between an AE emitted source with distance measured. Figs. 23 and 24 look at a tree rule based system between an AE emitted source and a measured force, where Fig. 25 shows the low force relationship, and Fig. 25 shows the high force relationship.

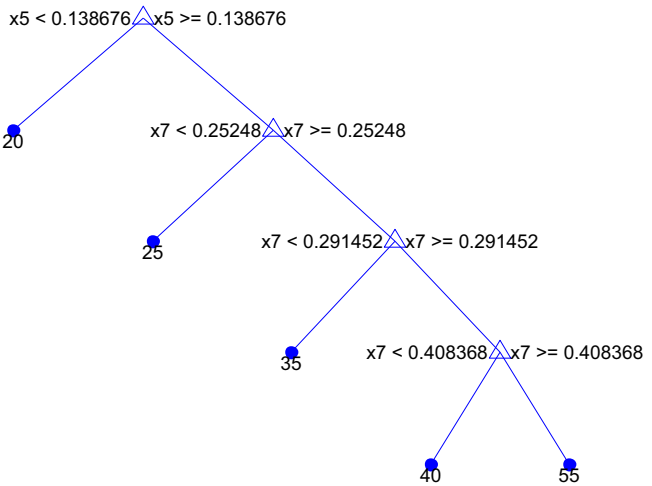

Fig. 23. Tree based rule system for low force classifications.

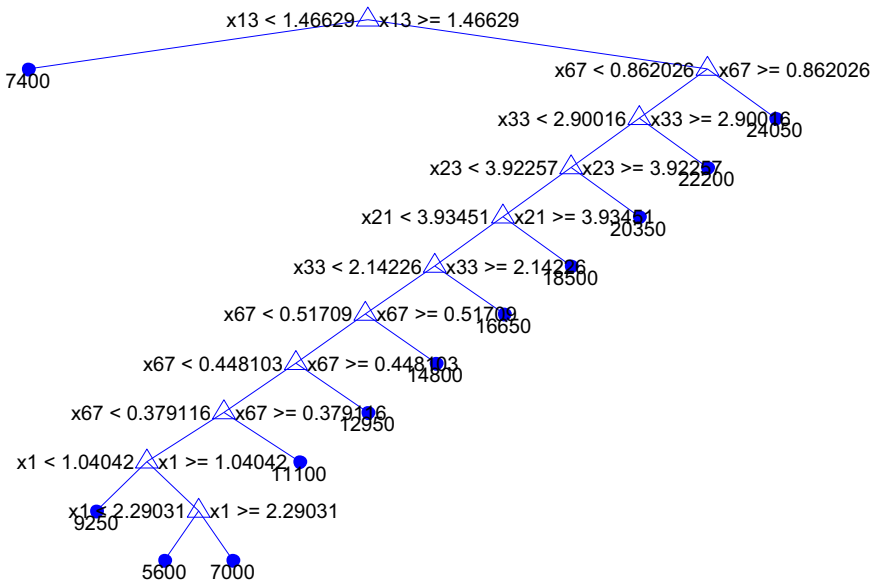

Fig. 24. Tree based rule system for high force classifications.

The three decision process mechanism works similar to the flight management seen on the US Space Shuttle where two decision discriminators agree, and the other one may not. The confidence of classification is based on two agreeing discriminators. Agreement is made by how close the classifications are to the reference data and determines the weighted amount given to the final classification. For this example, the model is supplied with 5 similar pencil calibrations (pencil break against the recorded AE event) and these are translated into rich windowed amplitude and time information. These 5 rich summaries (excluding any outliers) are averaged and a force and distance is given as output. This model can be used to calibrate both forces and distance less than and greater than that of pencil calibrations. The output from the Simulink model can be seen from Figs. 25 and 26 where the 5 input calibrations can be seen against their calculated average amounts. It is possible that more calibration data can be made to the 3 decision classifiers in the form of similar experimental data bolstering further AE calibration data.

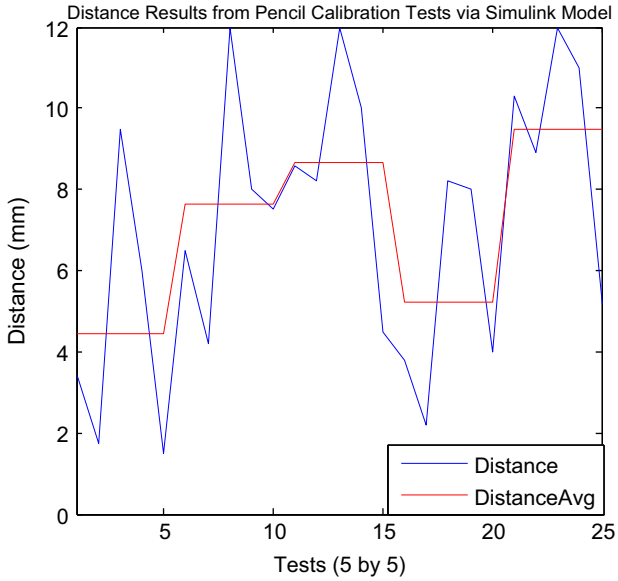

Fig. 25. Results from the distance module of Simulink AE calibration model.

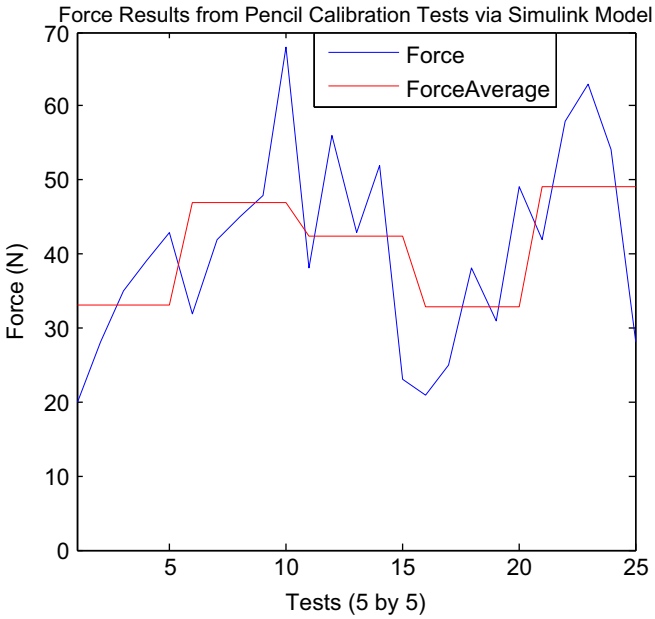

Fig. 26. Results from the force module of Simulink AE calibration model.

7.2. Simulink model for AE calibration against different material interactions

Figs. 27 and 28 display the AE calibration results against different material interactions through single grit scratch tests.

Both the results displayed in Figs. 27 and 28 give a 100% classification in that the technique of representing AE in both the time and frequency domains gives a good discriminator for both classification techniques. These two technologies are therefore realised in a second Simulink model segregating the four materials: EN8 Steel, Inconnel 718, CMSX4 and MARM-002.

Similar to Fig. 20, Fig. 29 displays the flow process for identification of different material AE signals emitted from SG tests which were measured at the same distance and same intensity of force throughout the tests. Fig. 30 displays an extension to the simulation displayed in Fig. 20 where the decision realisation in Fig. 30 was implemented into a Simulink model. This simulation uses two decision agreeing systems for an overall classification (the same technologies of NNs and fuzzy clustering NNs as seen in Fig. 20 were used to make the material associations).

8. Discussion of results

The AE sensor used during the trials was a Physical Acoustic Corporation® PAC WD (wide band) sensor. Table 7 lists each individual AE sensor characteristics. For the tests carried out in this work the sensors were set to V/μbar.

The detected signals from the AE sensors (see Table 7 for sensor characteristics) were passed through pre-amplifiers with a gain of 100(40 dB). A threshold dB pick-up setting (software) of 40 dB was used for SG tests. From carrying out earlier test

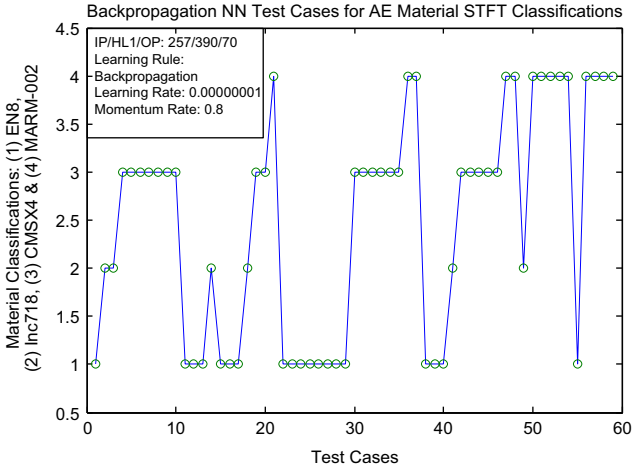

Fig. 27. NN results for different materials classifications.

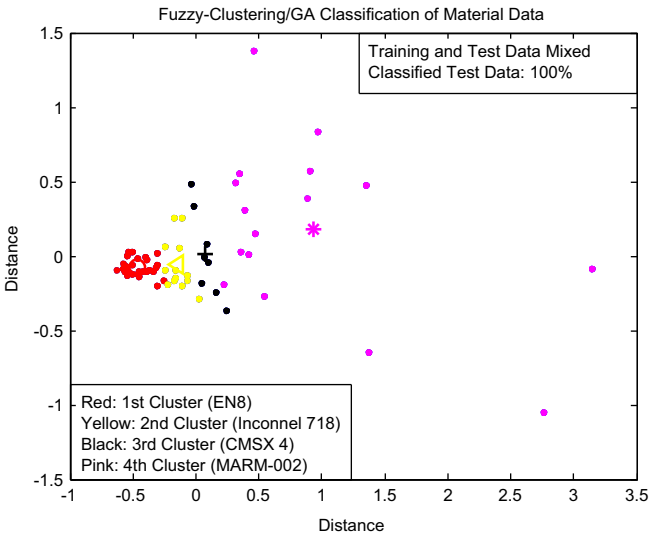

Fig. 28. Fuzzy-C/GA results for different materials classifications.

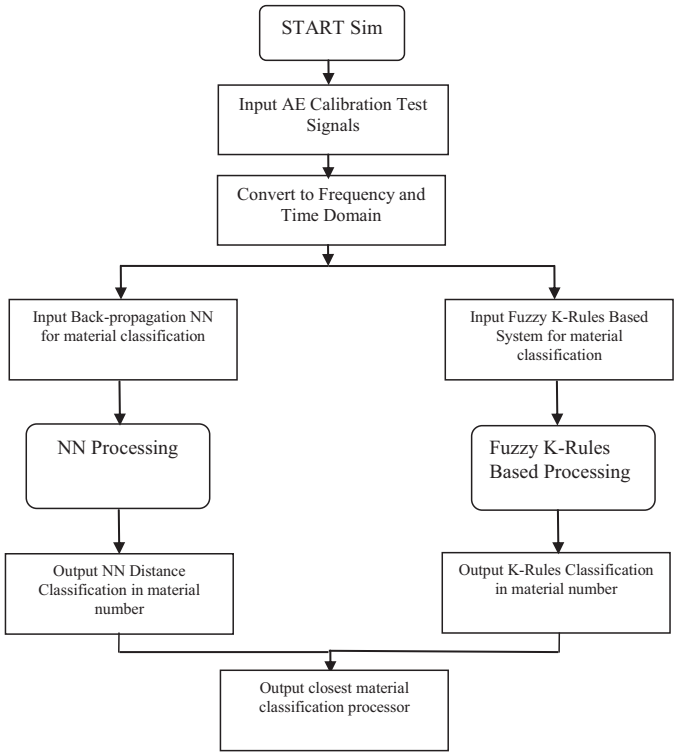

Fig. 29. Flow chart for material AE classification system.

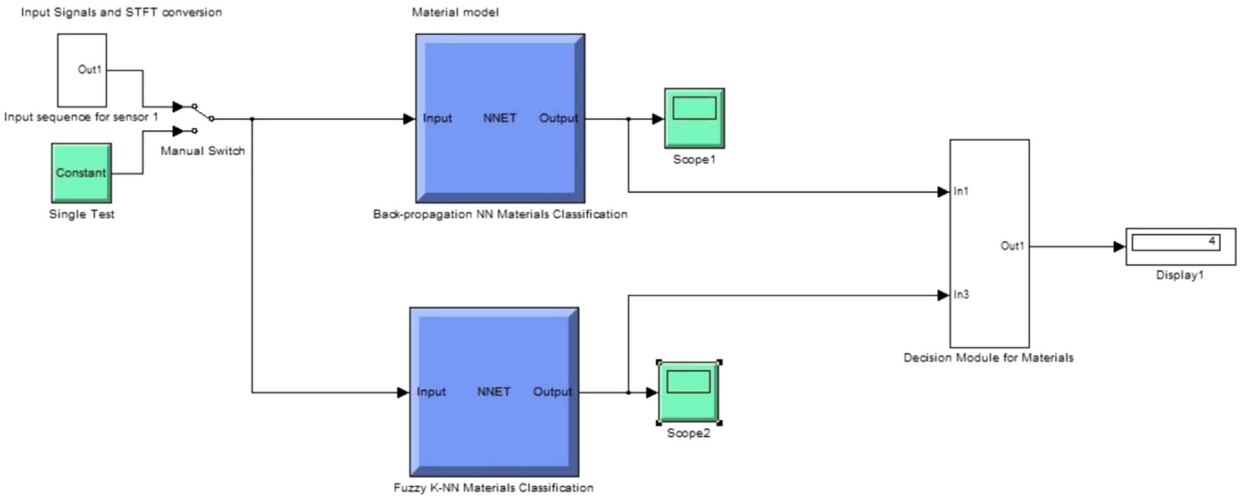

Fig. 30. AE calibration Simulink model for different materials classifications.

Table 7
Main specifications of AE sensors.

PAC WD SENSORS (1–3)	Sensor number/date	Construction	Sensor drive capability	Dimensions (dia.*ht.)	Peak sensitivity	Operating freq range (kHz)
	1) AL04/(17/11/04) 2) AL05/(17/11/04) 3) AL19(11/12/02)	Differential	Up to 100 m with w/RG-58 AU cable	17*16 mm	-63.21 (dB ref 1 V/μbar)	80–1000

trials and verifying the signal AE acquisition system it was possible to configure the sensor systems to the correct reference level to gain the phenomenon frequency response. This point is critical for any calibration system in that the noise level settings for amplification need to be taken into consideration when calibrating AE sources on a daily basis. The pre-amplifier also minimises or even eliminates mechanical and acoustical background noise that exits at low frequency, which is up to and including 20 kHz.

In reviewing the results presented in the last section it is possible to see that the results are inspiring for such a proposed AE standard. Future work would involve more tests to see how much different calibrations vary on a daily basis and whether it is necessary to increase the number of pencil break calibrations from five to ten to get a richer spread of calibration. If however there are large differences then more suitable and reliable methods of calibration are required such as an automatic pencil break method with specially designed apparatus as seen in works [9,10]. Or the combination of varying AE with respect to distance for pencil break and solenoid tests as seen in the statistical section.

The results provided by both simulation models give good confidence to the proposed technique in that the results were both accurate and verified against actual statistical experimental data. Looking at the given results it is possible to see that the proposed AE calibration method can give good confidence in correlating against force, distance and different material interactions.

This method has certainly pushed forward a possible automatic calibration method for AE measurement and therefore gives a novel approach to how such condition monitoring systems may look like in the future.

9. Conclusions

The experiments discussed within this paper were designed to investigate the correlations of force and distance based on the measured AE event occurrence. Such experimental tests displayed different techniques to segregate the different features obtained during different prolonged stresses in terms of AE measurements against different forces and distances. There are many questions to address in obtaining an internationally recognised standard for AE.

This paper takes a lot of previous works [1,2,7,8] and advances it to achieve a possible AE calibration method for condition monitoring. Also the paper displays where further work can be carried out in investigating different materials looking at different facets of material fracture. Previous works [1,2,7,8] looked at different signal properties; however as stated in [1,2] the first harmonic energy source of the phenomena is considered to be the most useful and as such was predominately used in the experiments discussed in this paper.

Different single grit tests were carried out displaying different intensities of force and distance; however for different material interaction tests the force and distance from the sensor were maintained throughout the tests giving balanced comparisons. The time series information was identified as enough to discriminate AE sources in terms of force and distance; however when faced with different materials both the time–frequency representations were necessary also. Within the work displayed in this paper it is possible to use both technologies to discriminate between force and distance, and for different materials. In the final parts of this work such tests were realised with intelligent models and simulations giving a more realistic realisation for such a proposal.

Varying distance AE intensities from pencil break and solenoid hit tests (reference Acoustic Emission Statistical tests in Section 4.7) the mechanical part of a proposed automated AE calibration system can be obtained.

The results displayed in Figs. 24 and 25 display high accurate output for a proposed AE calibration simulation. Both correlated distance and force were accurately associated with input AE signal phenomena. Figs. 26 and 27 also display accurate output of a two classifier system for distinguishing between different materials through extracted AE phenomena. This is where the same force and distance were exerted during different material SG tests.

The classification and simulation results are further reinforced by the AE statistical analysis which displays the significance of amplitude intensity correlated to both distance and force where the time to zero for the 5 max and 5 min points windowed along the extracted AE signal gives further verification in terms of phenomenon distance.

Such individual and simulation based results display the real possibility of an industrial AE calibration system to be used in various forms of condition monitoring and ultimately, form the basis for an accepted standard of AE sensor technologies.

References

[1] H. Hatano, T. Chaya, S. Watanabe, K. Jinbo, Reciprocity calibration of impulse responses of acoustic emission transducers, IEEE Trans. Ultrason., Ferroelectron., Freq. Control 45 (5[12]) (1998) 1221–1228.
[2] T. Yan, P. Theobald, B.E. Jones, A conical piezoelectric transducer with integral sensor as a self-calibrating acoustic emission energy source, Ultrasonics 42 (2004) 431–438.
[3] G. Byrne, Tool Condition Monitoring (TCM) – the status of research and industrial application., Ann. CIRP 48 (2) (1995) 541–567.
[4] K.M. Holford, Acoustic emission – basic principles and future directions, Strain 36 (2) (2000) 51–54.
[5] D.R. Natarajan, Investigation on the use of multiple acoustic emission sensors to detect process disturbances in machining, Diss. University of Nottingham, 2004.
[6] M. Barbezat, A.J. Brunner, et al., Acoustic emission sensor properties of active fibre composite elements compared with commercial acoustic emission sensors, Sensors Actuators a-Phys. 114 (1) (2004) pp13–pp20.
[7] T. Yan, P. Theobald, B.E. Jones, A self-calibrating piezoelectric transducer with integral sensor for in situ energy calibration of acoustic emission, NDT&E Int. 35 (2002) 459–464.

[8] N. Godin, S. Huguet, Gaertner, L. Salmon, Clustering of acoustic emission signals collected during tensile tests on unidirectional glass/polyester composite using supervised and unsupervised classifiers, NDT&E Int. 37 (2004) 253–264.
[9] J. Griffin, X. Chen, Multiple classification of the acoustic emission signals extracted during burn and chatter anomalies using genetic programming, Int. J. Adv. Manuf. Technol. 45 (11–12) (2009) 1152–1168.
[10] L. Qiang, Pattern recognition of grinding defects and assessment strategies of grinding (Ph.D. thesis), University of Nottingham, School of M3, 2004.
[11] R.M. Fisher, J.S. Lally, Can. J. Phys., CJPHA 45 (2, Part 3) (1967) 1147–1159.
[12] A.S. Tetelman, R. Chow, Acoustic Emission Testing and Microcracking Processes, 505, ASTM Special Technical Publication, 1972.
[13] R.Y. Chiou, S.Y. Liang, Dynamic modeling of cutting acoustic emission via piezoelectric actuator wave control, Int. J. Mach. Tools Manuf. 40 (5) (2000) 641–659.
[14] A.A. Pollock, Loading and stress in acoustic emission testing., Mater. Eval. 62 (3) (2004) 326–333.
[15] T. Boczar, M. Lorenc, Time–frequency analysis of the calibrating signal generated in the Hsu–Nielsen system, Phys. Chem. Solid State 7.3 (2006) 585–588.
[16] J. Griffin, X. Chen, Characteristics of the acoustic emission during horizontal single Grit scratch tests – Part 1 characteristics and identification, Int. J. Abras. Technol., Spec. Issue on: "Micro/Meso Mechanical Manufacturing (M4 Process)." 1 (4) (2009).
[17] X. Chen, J. Griffin, Q. Liu, Mechanical and thermal behaviours of grinding acoustic emission, Int. J. Manuf. Technol. Manage. (IJMTM) 12 (1–3) (2007) 184–199.
[18] S. Kalpakjian, S.R. Schmid, Manufacturing Process for Engineering Materials, Prentice-Hall, 2003, pp. 510–520, ISBN 0-13-040871-9.
[19] T. Opoz, X. Chen, Experimental investigation of material removal mechanism in single grit grinding, Int. J. Mach. Tools Manuf. 63 (2012) 32–40.
[20] B. Sick, On-line and indirect tool wear monitoring in turning with artificial neural networks: a review of more than a decade of research, Mech. Syst. Sign. Process. 16 (2002) 487–546.
[21] D.D. Rumelhart, G.E. Hinton, R.J. Williams, Learning representations by back-propagating errors, Nature 323 (1986) 533–536.
[22] J. Griffin, X. Chen, Characteristics of the acoustic emission during horizontal single Grit scratch tests – Part 2 classification and grinding tests, Int. J. Abras. Technol.- Spec. Issue on: "Micro/Meso Mechanical Manufacturing (M4 Process)." 1 (4) (2009).
[23] Xiaoli Li, Tool wear monitoring with wavelet packet transform-fuzzy clustering method, Wear 219 (2) (1998) 145–154.
[24] A. Cuevas, M. Febrero, R. Fraiman, Cluster analysis: a further approach based on density estimation., Comput. Statis. Data Anal. 36 (2001) 441–459.
[25] R.L. Lawrence, A. Wright, Rule-based classification systems using classification and regression tree (cart) analysis, Am. Soc. Photogramm. Eng. Remote Sens. (2001) 1137–1142.
[26] D. Coppersmith, S.J. Hong, J.R.M. Hosking, Partitioning nominal attributes in decision trees, Data Min. Knowl. Discov. 3 (1999) 197–217.
[27] J. Hartigan, Statistical theory in clustering, J. Classif. 2 (1985) 63–76.

James Griffin received his BEng in 1995 from College Cardiff, University of Wales. From 1996 to 2003, he was a member of the Defence Evaluation Research Agency (DERA) on numerous projects; one that significantly used genetic algorithms/neural networks to control an Unmanned Aircraft Vehicle (UAV). While he was working for DERA/QinetiQ, he completed a second degree (BSc in Technology Biased towards Artificial Intelligence) from the Open University (1996–2001). After this James decided to pursue this line of technology and, he obtained a PhD from the Advanced Abrasive Technology Group at the University of Nottingham applying intelligent concepts to identify different grinding phenomena. Later he applied this knowledge to a Rolls Royce Fellowship at the University of Nottingham working on a one machining process to manufacture a super-alloy turbine disk. James decided to broaden his technological knowledge in becoming Senior/Principal Engineer in simulation and modelling of missile systems for MBDA UK (formally known as BAe Dynamics). With this useful knowledge and skills in simulation and modelling James returned back to his true engineering interests as an Assistant Professor at the University of Chile working in advanced control and manufacture.